Molecular Beam Epitaxy of Layered Group III Metal Chalcogenides on GaAs(001) Substrates

Sergey V. Sorokin [1,*], Pavel S. Avdienko [1], Irina V. Sedova [1], Demid A. Kirilenko [1], Valery Yu. Davydov [1] , Oleg S. Komkov [2] , Dmitrii D. Firsov [2] and Sergey V. Ivanov [1,*]

[1] Ioffe Institute, 26 Politekhnicheskaya, 194021 St. Petersburg, Russia; avdienko.pavel@gmail.com (P.S.A.); irina@beam.ioffe.ru (I.V.S.); demid.kirilenko@mail.ioffe.ru (D.A.K.); valery.davydov@mail.ioffe.ru (V.Y.D.)

[2] St. Petersburg Electrotechnical University "LETI", 5 Prof. Popova, 197376 St. Petersburg, Russia; okomkov@yahoo.com (O.S.K.); d.d.firsov@gmail.com (D.D.F.)

[*] Correspondence: sorokin@beam.ioffe.ru (S.V.S.); ivan@beam.ioffe.ru (S.V.I.)

check for updates

Abstract: Development of molecular beam epitaxy (MBE) of two-dimensional (2D) layered materials is an inevitable step in realizing novel devices based on 2D materials and heterostructures. However, due to existence of numerous polytypes and occurrence of additional phases, the synthesis of 2D films remains a difficult task. This paper reports on MBE growth of GaSe, InSe, and GaTe layers and related heterostructures on GaAs(001) substrates by using a Se valve cracking cell and group III metal effusion cells. The sophisticated self-consistent analysis of X-ray diffraction, transmission electron microscopy, and Raman spectroscopy data was used to establish the correlation between growth conditions, formed polytypes and additional phases, surface morphology and crystalline structure of the III–VI 2D layers. The photoluminescence and Raman spectra of the grown films are discussed in detail to confirm or correct the structural findings. The requirement of a high growth temperature for the fabrication of optically active 2D layers was confirmed for all materials. However, this also facilitated the strong diffusion of group III metals in III–VI and III–VI/II–VI heterostructures. In particular, the strong In diffusion into the underlying ZnSe layers was observed in ZnSe/InSe/ZnSe quantum well structures, and the Ga diffusion into the top InSe layer grown at ~450 °C was confirmed by the Raman data in the InSe/GaSe heterostructures. The results on fabrication of the GaSe/GaTe quantum well structures are presented as well, although the choice of optimum growth temperatures to make them optically active is still a challenge.

Keywords: III–metal chalcogenides; 2D materials; GaSe; InSe; GaTe; quantum wells; molecular beam epitaxy; GaAs(001) substrate; photoluminescence; Raman spectroscopy; transmission electron microscopy; X-ray diffraction

1. Introduction

Layered two-dimensional (2D) group III metal chalcogenides (MCs) (GaSe, GaTe, InSe, and others) are still of strong interest for the development of novel high-performance semiconductor devices due to their unique electronic and optical properties [1–3]. In particular, these materials have attracted great attention for the fabrication of field-effect transistors [4], solar cells [5,6], high-efficient photodetectors, and gas sensing devices [7,8]. InSe has significant potential for using in thermoelectric applications [9]. In addition, GaSe and GaTe are the nonlinear optical crystals and can be used for terahertz (THz) wave generation [10,11].

One of the main reasons for intensive studies of 2D layered materials is that they exhibit different properties in a few-layer and bulk forms [12–14], providing an additional degree of freedom in the development of electronic and optical devices. To date, most of the 2D layered semiconductors and

heterostructures based on them are either prepared by mechanical exfoliation from bulk crystals or grown by chemical (physical) vapor transport (CVT, PVT) or chemical vapor deposition (CVD) techniques [15]. Although the sophisticated multilayered structures consisting of various 2D materials bonded to each other via weak van der Waals forces can be produced using the scotch-tape method ("realizing the idea that 2D materials can be stacked as Lego blocks" [16]), this technology can hardly be used for the fabrication of commercial devices. At the same time, the use of epitaxial growth techniques, in particular molecular beam epitaxy (MBE), potentially allows fabrication of 2D thin films and heterostructures with abrupt interfaces and a uniform wafer-scale film thickness. Moreover, when the epitaxial growth proceeds via van der Waals forces (the so-called van der Waals growth mode), the 2D materials can be grown on highly-mismatched substrates, even when symmetries of the grown film and substrate differ [17], which is important for integration with conventional 3D semiconductors.

The abilities of MBE for the 2D device fabrication were recently demonstrated by Yuan et al. [18], who fabricated highly efficient photodetector arrays with external quantum efficiency up to 62% and photoresponse time of 22 μs using few-layer GaTe films grown by MBE on 3-inch Si wafer. The layer-by-layer growth mode has also been achieved in MBE of GaSe on mica and Si(001) substrates [19]. Wafer-scale $GaTe_xSe_{1-x}$ films, grown by MBE on freshly cleaved mica or cleaned silicon substrates, were also reported by Liu et al. [20]. Thus, the opportunity of realization of high-quality films and heterostructures composed of 2D group III MCs by MBE has already been proved. However, due to a number of polytypes and additional phases, the synthesis of defect-free films is still a problem. It is also complicated by the much lower substrate temperatures used in MBE as compared to other epitaxial techniques.

In this paper, we present the results on MBE growth of thin films of III–VI layered MCs (GaSe, InSe, and GaTe) and their heterostructures on conventional GaAs(001) substrates, as well as studies of their structural and optical properties. The use of a combination of conventional and two-dimensional semiconductors in a single heterostructure allows expanding the range of potential applications. Although the first publications on MBE growth of group III MCs date back to the early 1990s [21,22], there are many gaps in understanding growth mechanisms, and there is still no universal recipe for the growth of high-quality optically active structures based on these layered materials.

2. Materials and Methods

2.1. Materials Properties

The layered chalcogenides of the MX type, where X = (Se, Te) and M = (Ga, In), consist of vertically ordered layers which are bonded together by weak van der Waals forces, and each layer contains four covalently-bonded atomic sheets in the sequence X-M-M-X.

GaSe is one of the most studied 2D layered III–VI semiconductors, which has an indirect bandgap in the visible range with an energy of ~2 eV at T = 300 K, which is only 25 meV lower than the direct bandgap [1,23–25]. GaSe films can crystallize in different polytypes (β, ε, γ, and δ), which differ from each other by stacking sequence of the layers [26]. γ-GaSe has a rhombohedral crystal lattice with the R3m space group and the lattice parameters a = 3.75 Å and c = 23.92 Å, whereas β-, ε, and δ-GaSe have a hexagonal crystal lattice with P6₃/mmc, P6m2, and P6₃mc space groups, respectively [26]. Both hexagonal β- and ε-GaSe polytypes have the same lattice parameters a = 3.750 Å and c = 15.94 Å [1]. The formation of one or another polytype depends on both the technique and growth conditions used for the GaSe film fabrication (see, e.g., [27]). In particular, GaSe layers grown by MBE are usually of ε- or γ-polytype [19,28–30]. However, some domains of β-polytype were also observed in GaSe films grown by MBE on MoS_2 cleaved surfaces [31]. The thickness of one monolayer (or, more accurately, one tetralayer (TL)) GaSe is ~0.8 nm for all polytypes.

As with many other 2D materials, GaSe is unstable and oxidizes in ambient conditions, which leads to a gradual degradation of its optical properties [32–34]. The Raman spectroscopy analysis showed that GaSe decomposes into Ga_2Se_3 and amorphous Se during oxidation [32,34]. Moreover, during the

prolonged storage in air, the GaSe surface also undergoes visible transformations [35]. The oxidation of GaSe is a rapid process with a monolayer reaching an oxidized state almost immediately after exposure to air [34]. To prevent the atmospheric oxidation, the surface passivation using 50-nm-thick Al_2O_3 layer was proposed [33]. The effective protection is even more important if the grown GaSe layer consists of a large number of nanometer-scale nanoplatelets.

InSe is a direct-gap semiconductor with E_g = 1.25–1.3 eV at room temperature in the bulk form; however, there is some spread in the bandgap values reported in the literature for various polytypes [1,36–39]. There are three polytypes of layered InSe (β, γ, and ε), which differ in the symmetry and stacking sequence of the layers [1,36]. The crystal space groups of the respective InSe polytypes are the same as in the case of GaSe. The lattice constant as well as the distance between two neighboring layers are nearly the same for all polytypes: a ≈ 4.0 Å [36,40–42], d ≈ 0.84 nm [1,36,39,43]. The ε- and γ-InSe are the most widely studied InSe polytypes with a hexagonal unit cell. These two hexagonal phases are hardly distinguishable, as they exhibit a similar composition of the unit cell and the same lattice parameters. The γ-polytype has a rhombohedral unit cell with the lattice parameter c = 24.96 Å, which is 1.5 times larger than that of β-InSe and γ-InSe.

In contrast to the most commonly studied 2D materials, the direct-gap semiconductor GaTe (E_g = 1.7 eV in a bulk form at T = 300 K [1]) has a monoclinic crystal structure in the space group C2/m, the symmetry of which is less than hexagonal lattice structure, with lattice parameters a = 17.32 Å, b = 4.05 Å, c = 10.54 Å and β = 104.4° [1]. Low-symmetry 2D materials show significant in-plane anisotropy in their electrical, optical, and thermal properties [44]. Two-thirds of the Ga-Ga bonds in GaTe are perpendicular to the layer and the rest are parallel to the layer. The thickness of each GaTe layer is also ~0.8 nm [1,18,45]. A metastable hexagonal phase for GaTe has also been reported with the lattice parameters a = 4.06 Å and c = 16.96 Å (space group P6₃/mmc) [46].

Similar to GaSe, GaTe is also characterized by a very high oxidation rate in air, which results in a gradual degradation of its optical properties. Moreover, recently Fonseca et al. demonstrated that GaTe exposure to air leads to a significant restructuring of the conduction band due to the incorporation and chemisorption of oxygen to tellurium with subsequent transformation into a disordered GaTe–O_2 phase [47]. To prevent the atmospheric oxidation of the GaTe, the surface passivation with Al_2O_3 is required [33]. In this study, we stored the GaTe samples in vacuum. This method also substantially delays the degradation of optical properties, but, of course, is not practical for real-life applications.

2.2. Thin-Films Synthesis

Thin films of 2D-layered MCs were grown on epi-ready GaAs(001) substrates at a substrate temperature of T_S = 400–530 °C using a double-chamber MBE setup (SemiTEq, St. Petersburg, Russia). Standard Ga, In, and Te effusion cells as well as a Se valve cracking cell (Veeco, Plainview, NY, USA) with the cracking zone temperature T_{Se}(cr) = 500 °C were used as molecular beam sources. The samples were grown either directly on thermally cleaned GaAs substrate or on 200-nm-thick GaAs buffer layer grown in a separate III–V growth chamber and transferred to the III–VI chamber through vacuum. In the former case, the substrates were first heated to T_S ~ 600 °C without an As overpressure to remove the surface oxide layer, which was controlled by reflection high energy electron diffraction (RHEED) measurements, and then the substrate was cooled to the deposition temperature. In the latter case, after the transferring of GaAs buffer to the III–VI growth chamber the substrate temperature was gradually increased to the growth temperature with the rate ~20 °C/min. When the substrate temperature was stabilized at a given value, the growth was started as soon as possible to avoid the reaction between the substrate surface and residual Se. In the case when the initial deposition temperature was below 500 °C, we used also the main shutter for additional protection of GaAs(001) growth surface. The VI/III flux ratio was controlled by measuring the beam equivalent pressures (BEPs) of the respective elements at the substrate position by using a Bayard-Alpert ion gauge. The growth parameters of GaSe and GaTe epitaxial layers are outlined below. The details of MBE growth of specific III–VI MCs and heterostructures are given in the corresponding parts of the paper.

2.3. Characterization

The samples were characterized by cross-sectional transmission electron microscopy (TEM), scanning electron microscopy (SEM), X-ray diffraction (XRD), Raman spectroscopy, and photoluminescence (PL) spectroscopy techniques. The growth of all layers and heterostructures was monitored in situ by using RHEED.

The Raman measurements were performed both at room and liquid nitrogen temperatures using a T64000 (Horiba Jobin-Yvon, Lille, France) spectrometer equipped with a confocal microscope. The line at λ = 532 nm of Nd:YAG laser (Torus, Laser Quantum, Inc., Edinburg, UK) and the 514.5 and 488 nm lines of Argon laser (Spectra-Physics, Inc., Mountain View, CA, USA) were used as the excitation sources. The laser power on the samples was as low as ~25–80 μW with a spot size of ~1 μm in diameter. The room-temperature PL spectrum of the GaSe/GaAs(001) layer was also measured using the described experimental setup.

The low-temperature PL measurements of the GaTe/GaAs(001) layer as well as temperature-dependent PL measurements of the InSe/GaAs(001) layer were carried out using experimental setup based on a Vertex 80 Fourier-transform infrared (FTIR) spectrometer (Bruker, Germany) equipped with a Si photodiode detector and a CaF_2 beam splitter as described in Ref. [48]. The samples were placed into a Janis CCS-150 closed-cycle helium cryostat with a LakeShore 325 temperature controller, and the luminescence was extracted via CaF_2 window and lenses. A 405 nm violet diode laser SSP-DHS-405 was used as the excitation source.

Micro-PL spectra of the GaSe/GaAs(001) layers were measured within the 10–110 K temperature range in a He-flow ST-500-Attocube cryostat. The spectra were recorded using a cooled CCD camera; the laser line at λ = 405 nm of CUBE laser (Coherent) was used as the excitation source. The laser power density on the sample was below 1 W/cm^2.

Time-resolved measurements of the luminescence in ZnSe/InSe/ZnSe structures were performed at T = 77 K. The samples were excited by 405 nm radiation of CUBE laser (Coherent) with pulses of 45 ps duration at a repetition rate of 1 MHz.

The cross-section transmission electron microscopy (TEM) measurements were carried out using Jeol JEM-2100F microscope (the accelerating voltage 200 kV; the pixel resolution 0.19 nm). The samples were prepared by the standard procedure, i.e., by mechanical polishing with subsequent thinning by etching with Ar$^+$ ions (4 keV). D2 Phaser powder diffractometer (Bruker, Germany) was used for the XRD measurements. The SEM measurements were used to estimate the thickness of the layers and to study the surface morphology of the grown layers. Both plan-view and cross-section SEM images of the grown samples were obtained by using CamScan microscope.

3. Results and Discussion

3.1. MBE Growth of GaSe/GaAs(001)

The basic peculiarities of GaSe MBE growth on GaAs substrates were established in the 1990s [49–53]. In the last decade, a new surge of interest in GaSe (and, of course, in other 2D layered materials) has arisen because of the discovery of graphene in 2004 [54]. However, as already noted, no recipe for growing the high-quality optically active structures was developed. The GaAs(111)B substrate seems to be a natural candidate for the growth of GaSe layers because of a relatively low lattice-mismatch of ~6% [21]. Indeed, the MBE growth of GaSe on a hexagonally symmetric, three-dimensional GaAs(111)B substrate has been shown to be free of the critical thickness problem, which is of a great importance for potential device applications [21,49]. However, the growth of GaSe on GaAs(111) is hardly achieved at growth temperatures above 500 °C, since GaSe is re-evaporated from the growing surface due to a weak van der Waals force [49]. As a result, no PL emission from the GaSe films was detected due to its rather poor crystallinity.

The van der Waals growth mode was also realized in MBE growth of GaSe/GaAs(001) at low temperatures $T_S \approx$ 400 °C, with the *c* axis of the growing GaSe layer oriented along the normal to

the substrate surface [49]. At higher growth temperatures ($T_S > 500$ °C), the nucleation of GaSe on the GaAs(001) surface occurs through the formation of transitional submonolayers with a chemical bonding between the substrate and the layer [49,50].

Both spiral and island growth modes were reported for GaSe layers grown by MBE on different substrates [31,52,55,56]. In particular, the spiral pyramid-like morphology has been reported for the GaSe/GaAs(001) layers grown by MBE at low $T_S \approx 400$ °C [55]. The evolution of GaSe morphology with growth time, observed by using the atomic force microscopy (AFM) technique, has been explained by the realizing of screw-dislocation-driven (SDD) growth mode, which is typical for the growth of 2D materials [57]. We did not use AFM in this study systematically; however, our data on GaSe/GaAs(001) layers are in a good agreement with those of other research groups. Thus, the existence of SDD growth mechanism in our GaSe layers grown at $T_S \approx 400$ °C directly on GaAs(001) substrates is highly likely. To grow uniform large-area layered materials with a controlled number of layers the SDD growth mode should definitely be avoided. According to Nie et al. [57], to do this, both the growth rate and the chalcogen-to-metal ratio need to be limited during deposition, and these parameters are especially important at the early nucleation and growth stages. The quality of the substrate also plays a significant role, so the use of a GaAs buffer layer along with a low growth rate as well as a choice of appropriate growth conditions could, in principle, provide the layer-by-layer growth mode in MBE of layered chalcogenides. The need for a low deposition rate for the formation of flat GaSe layers was confirmed by Yuan et al. [19], who demonstrated layer-by-layer growth of GaSe on mica and Si(001) substrates with a growth rate in the range 0.3–0.8 nm/min. The importance of a very low GaSe deposition rate ($r_{GaSe} \approx 0.2$ nm/min) for the controllable growth of high-quality atomically thin GaSe layers was also demonstrated by Chen et al. [58].

The need for a low Se/Ga flux ratio is confirmed by the experimental fact that the optimum conditions for the MBE growth of GaSe on GaAs(001) substrates correspond to the nearly stoichiometric ratio between the adsorbed Ga and Se adatoms on the growth surface [30,49,50]. An analysis of the available literature data, taking into account the dependence of Se incorporation coefficient on both substrate and cracking zone temperatures of the Se valve source [59], shows that the stoichiometric conditions can be estimated as corresponding to P_{Se}/P_{Ga} (BEP) ~ 12 and ~ 25 at $T_S = 400$ °C and 500 °C, respectively, if standard Ga and Se valve cracking cells with $T_{Se}(cr) = 500$ °C are used as molecular beam sources [28]. In our analysis, we used the measured P_{Se}/P_{Ga} (BEP) flux ratios needed to obtain a relatively smooth GaSe surface at various temperatures (350–450 °C) from [30], where a Se valve cracking cell with $T_{Se}(cr) = 950$ °C was applied as a Se source, as well as data on GaSe layers grown by MBE using standard Ga and Se cells [29,49–51]. The estimated dependence of the R = P_{Se}/P_{Ga} (BEP) ratio, corresponding to the stoichiometric conditions on the growth surface for various T_S, is presented in Figure 1. One should note that it is difficult to associate the Se/Ga BEPs ratios taken from different sources with the stoichiometric growth conditions, especially keeping in mind that there is some uncertainty in determining the real temperature of epitaxial growth. However, it can be assumed that the formation of gallium droplets on the GaSe surface is the only reliable indicator of Ga-rich MBE growth conditions. The points corresponding to the GaSe layers grown at different T_S with and without Ga droplets on the growth surface are shown in Figure S1. The obtained data confirm the correctness of our estimations. It follows directly from the dependence in Figure 1 that the stoichiometry on the growth surface at a fixed T_S can be controlled either by adjusting the opening of the Se valve or by changing the cracking zone temperature $T_{Se}(cr)$ of the valve Se cell. In the latter case, the change in the ratio of the Se and Ga adatoms on the growth surface occurs due to a change in the Se sticking coefficient.

The growth of GaSe on GaAs(001) substrates was initiated by the simultaneous opening of Ga and Se fluxes. One should note, the RHEED observations showed that initial (2 × 4)As reconstruction of the GaAs(001) buffer layer changed to the (2 × 1)Se-terminated one while rising the substrate temperature under Se exposure or unintentionally if there was a Se background in the growth chamber. The growth

parameters as well as the thicknesses of the GaSe epitaxial layers are outlined in Table 1. The presence or absence of a buffer layer in a particular structure is also indicated.
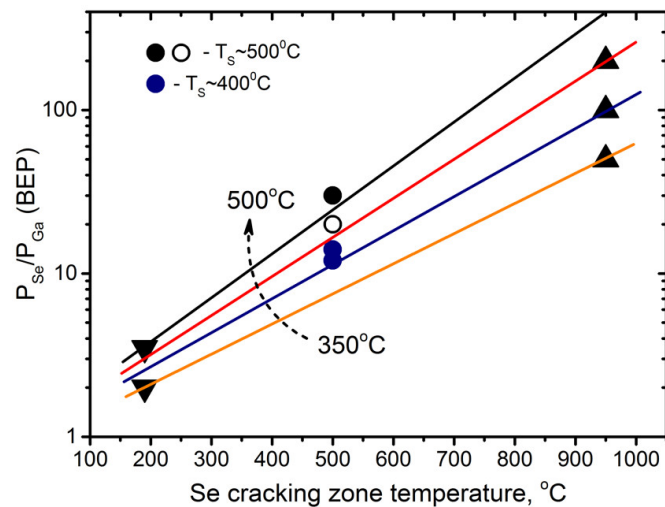

Figure 1. The calculated dependences of the P_{Se}/P_{Ga} (BEP) ratio corresponding to stoichiometric conditions on the GaSe growth surface at different T_S, marked in different colors ($T_S = 350$ °C, orange; $T_S = 400$ °C, blue; $T_S = 450$ °C, red; and $T_S = 500$ °C, black). The data of Lee et al. [30] are shown by filled triangles with the vertex pointing up ($T_{Se}(cr) = 950$ °C). The data on P_{Se}/P_{Ga} (BEP) flux ratios corresponding to nearly stoichiometric conditions for GaSe layers growth using standard Ga and Se cells are shown by filled triangles with the vertex pointing down. Our data on P_{Se}/P_{Ga} (BEP) flux ratio for the GaSe layers grown at $T_S = 400$ and 500 °C are shown by blue and black circles, respectively. GaSe layers with and without Ga droplets on the growth surface are indicated by the hollow and filled circles.

Table 1. The growth parameters of GaSe/GaAs(001) layers.

Layer	T_{Ga}; Ga flux (BEP)	Se/Ga Flux Ratio [1], (BEP/Real)	T_S, °C	Layer Thickness, nm (SEM)	Average Growth Rate [2], nm/min	Notes
#GS1	$T_{Ga} = 910$ °C; $P_{Ga} = 4.7 \times 10^{-8}$ Torr	Se/Ga (BEP) ~ 34; (Se/Ga ~ 3.9)	410	200	1.3	Se cracking zone temperature $T_{Se}(cr) = 450$ °C
#GS2	$T_{Ga} = 900$ °C; $P_{Ga} = 4.0 \times 10^{-8}$ Torr	Se/Ga (BEP) ~ 42; (Se/Ga ~ 4.8)	400	270	1.13	Se cracking zone temperature $T_{Se}(cr) = 450$ °C
#GS3	$T_{Ga} = 940$ °C (1st stage); $T_{Ga} = 920$ °C (2nd stage); $P_{Ga} = 9.0 \times 10^{-8}$ Torr (1st stage); $P_{Ga} = 6.0 \times 10^{-8}$ Torr (2nd stage)	Se/Ga (BEP) ~ 20/30; (Se/Ga ~ 1.6/1.2)	410—1st stage 500—2nd stage	360	~3	0.2-µm thick GaAs buffer layer; two-stage growth mode
#GS4	$T_{Ga} = 940$ °C; $P_{Ga} = 9.0 \times 10^{-8}$ Torr	Se/Ga (BEP) ~ 18–20; (Se/Ga ~ 0.9–0.95)	480	50	~1.4	Ga droplets on the surface with diameter ~200–300 nm
#GS5	$T_{Ga} = 954$ °C; $P_{Ga} = 1.25 \times 10^{-7}$ Torr	Se/Ga (BEP) ~ 12–13; (Se/Ga ~ 1)	410	300	5	0.2-µm thick GaAs buffer layer
#GS6	$T_{Ga} = 910$ °C; $P_{Ga} = 5.5 \times 10^{-8}$ Torr	Se/Ga (BEP) ~ 13–14; (Se/Ga ~ 1.1–1.2)	405	90	1.5	
#GS7	$T_{Ga} = 910$ °C; $P_{Ga} = 5.5 \times 10^{-8}$ Torr	Se/Ga (BEP) ~ 25; (Se/Ga ~ 1)	500	400	2.2	
#GS8	$T_{Ga} = 890$ °C; $P_{Ga} = 3.8 \times 10^{-8}$ Torr	Se/Ga (BEP) ~ 21; (Se/Ga ~ 1.6)	410	-	~1.0	rough growth surface

[1] The calculated Se/Ga ratios of the impinging atoms on the GaAs surface are given taking into account the growth temperature (T_S) and the cracking zone temperature of the valve Se source, influencing the Se sticking coefficient.
[2] The average growth rate was calculated using the layer thickness determined from SEM measurements and deposition time.

The surface morphology of the GaSe/GaAs(001) layers was analyzed by SEM. The plan-view images of the thick (>50 nm) layers grown at T_S ~ 400 °C and at different Se/Ga flux ratios with nearly the same growth rate of ~1.1–1.4 nm/min look quite similar: one can see a number of so-called "nanoplatelets" of different size and shape, randomly distributed on the relatively flat growth surface (Figure 2a,b). The similar surface morphology was observed in GaSe layers grown on GaAs(112) substrates at the same growth temperature T_S ~ 400 °C [28]. At the optimized conditions, where the adsorbed Ga and Se adatoms are close to stoichiometry, and the growth rate is relatively low, the RHEED pattern remained streaky for a long-time during MBE growth (Figure S2a). However, under strong Se-rich conditions the brightness of the RHEED pattern gradually decreased with increasing layer thickness, and the streaky reflections became wider and blurred. In some areas of the RHEED pattern, spots as well as Debye rings appeared, indicating a polycrystalline growth. The observed RHEED images are very similar to that reported in [30] for the GaSe layers grown on GaN/sapphire in Se-rich conditions, and reflect an increase in surface roughness as the layer grows, which can be induced by the formation of a multi-domain structure at the initial growth stage. We assume that the "growth window" in the case of MBE growth of GaSe using standard Ga and Se valve cracking cells as molecular beam sources is narrower than in the case of using standard Ga and Se effusion cells.
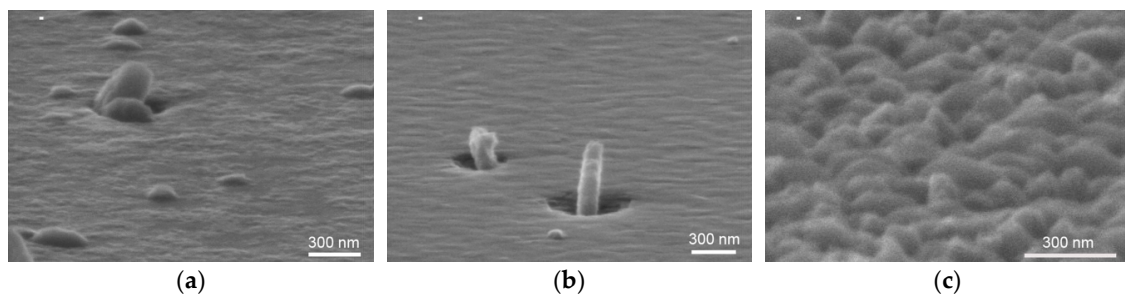

(**a**)　　　　　　　　　　　　　(**b**)　　　　　　　　　　　　　(**c**)

Figure 2. SEM images of the GaSe layers grown on the epi-ready GaAs(001) substrates at T_S ~ 400 °C. The Se/Ga (BEP) flux ratios and growth rates were the following: (**a**) Se/Ga (BEP) ~ 42, $r_{GaSe} \approx 1.13$ nm/min, sample *#GS2*; (**b**) Se/Ga(BEP) ~ 34, $r_{GaSe} \approx 1.3$ nm/min, *#GS1*; (**c**) Se/Ga (BEP) ~ 12–13, $r_{GaSe} \approx 5$ nm/min, *#GS5*. The thicknesses of the structures ranged within 200–300 nm. In the case of using standard Ga and Se valve cracking cell with $T_{Se}(cr) = 500$ °C as molecular beam sources, the stoichiometric Se/Ga ratio at $T_S = 400$ °C corresponds to the P_{Se}/P_{Ga} (BEP) ~ 12.

Although the Se/Ga flux ratio affects both the surface density of nanoplatelets and their size, the main parameter determining the surface morphology, in addition to T_S, is the Ga flux which controls the GaSe growth rate. The SEM image of the GaSe layer grown with a deposition rate of ~5 nm/min at T_S ~ 400 °C, as shown in Figure 2c, reveals a very rough surface of GaSe film despite the nearly stoichiometric flux ratio used. We suppose that the mobility of gallium atoms in this case is apparently insufficient for the formation of the flat layer morphology.

The cross-section TEM image of the GaSe layer grown at T_S ~ 400 °C with a low growth rate $r_{GaSe} \approx 1.13$ nm/min (sample *#GS1*) confirms the formation of a relatively flat layer with a nearly abrupt GaSe/GaAs(001) interface (Figure 3a). The thickness of the GaSe film is about 200 nm and relatively uniform. The inhomogeneous contrast of the image can be related to the high density of extended defects and a number of domains in the grown film. Figure 3b shows the high-resolution TEM image of a GaSe/GaAs(001) interface for the same layer. The rough boundary between GaSe and GaAs is likely due to a thermal cleaning of the GaAs(001) substrate in the absence of the As flux. One can clearly see the layered structure of GaSe. The observed interplanar spacing of the film is of ~0.8 nm, which is equal to the thickness of one tetralayer. The selected area electron diffraction (SAED) (Figure S3a) revealed that the layer has a predominantly rhombohedral structure, which corresponds to the γ-polytype. The formation of the γ-GaSe polytype is typical for the MBE grown GaSe/GaAs(001) layers, as reported previously [29,50]. The *c* axis of the GaSe layer is normal to the substrate/layer interface (Figure 3b). It is difficult to draw an unambiguous conclusion about the formation of any transition layer at the

GaSe/GaAs(001) interface from the TEM image shown in Figure 3b. Nevertheless, the existence of built-in electric fields generated at the GaSe/GaAs(001) heterointerface, as indicated by clearly observed Franz–Keldysh oscillations in the photoreflectance spectra [60], may indirectly indicate the formation of such layers at the initial growth stages. Another possible explanation is related to the diffusion of Se atoms into the GaAs substrate. The possibility of the formation of Ga_2Se_3-type intermediate layers at the GaSe/GaAs(001) interface was demonstrated by Dai et al. [29,61].
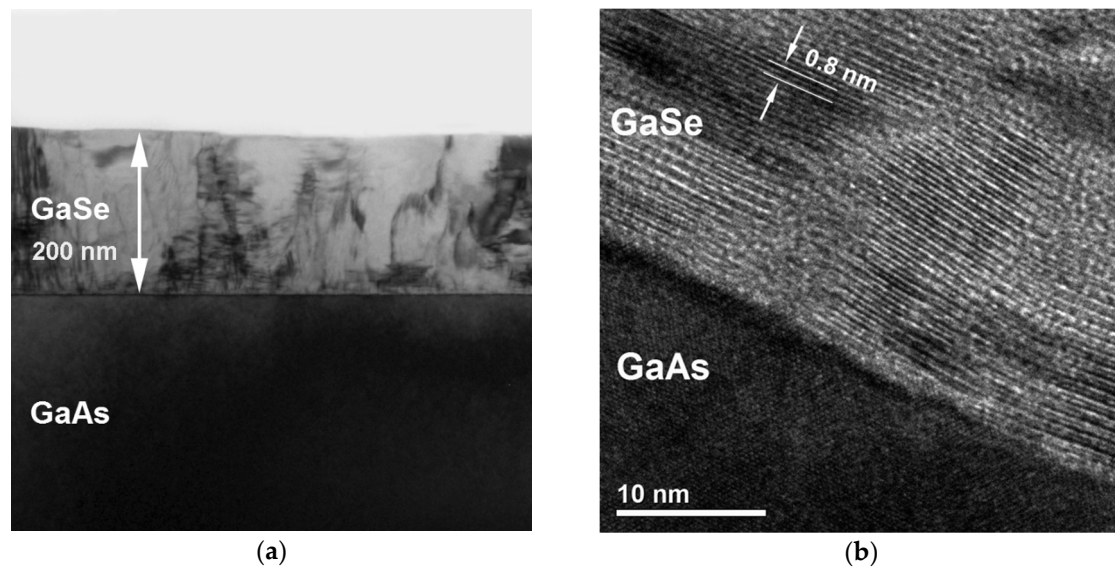
Figure 3. (**a**) Cross-section TEM image of the GaSe layer grown on the GaAs(001) substrate at T_S ~ 400 °C (Se/Ga(BEP) ~ 34) (sample #*GS1*); (**b**) high-resolution TEM (HRTEM) image of the GaSe/GaAs(001) heterointerface for the same layer.

With increasing T_S, the surface morphology of the GaSe/GaAs(001) layers became rougher. It should be noted that this tendency was also observed for the GaSe layers grown in a two-stage regime, i.e., for layers in which the initial GaSe layer was deposited at a low substrate temperature T_S ~ 400 °C. At T_S ~ 500 °C, no flat layer was observed; the structure comprised an array of nanoplatelets tilted toward both $[110]$ and $[1\overline{1}0]$ directions of the GaAs substrate (Figure 4a and Figure S4a) [49]. Despite a certain degree of disordering, due to the chemical interaction between the substrate and the growing layer, the *c* axis of GaSe nanoplatelets is predominantly oriented along the <111> directions of the GaAs substrate (Figure 4b). One can also see the formation of an intermediate layer near the GaSe/GaAs interface in some nanoplatelets, which leads to an additional layer tilt caused by a partial stress relaxation to accommodate the lattice mismatch between GaSe and GaAs, as previously reported by Kojima et al. [50]. Nevertheless, the areas where the GaSe domains start to grow with the *c* axis normal to the substrate/layer interface are retained (Figure S4b). The average growth rate of the GaSe layer shown in Figure 4 was as high as ~2.2 nm/min. The appearance of the clearly resolved spots on the streaked RHEED pattern reflected the disordering on the growth surface. Nevertheless, the RHEED pattern remained nearly streaky during all 3 h of growth, and the brightness of the RHEED pattern remained virtually unchanged with increasing layer thickness (Figure S2b). When the growth temperature was raised up to T_S > 530–540 °C, no growth of GaSe was observed even at a high Ga flux intensity.

For the GaSe layers grown at T_S ~ 400 °C with a Ga beam flux of $(4–6) \times 10^{-8}$ Torr, the growth rate estimated from the cross-section SEM images is nearly proportional to the impinging Ga flux, which reflects the growth of the layers with a relatively planar surface morphology (samples #*GS1*, #*GS2*, and #*GS6* in Table 1). However, for the layers with rough surface morphology grown at a high Ga beam flux, and for the layers consisting of a set of inclined nanoplatelets (#*GS7*), the average growth

rate estimated from cross-section SEM images is higher than the expected one from the impinging Ga flux, which confirms the growth of discontinuous layers.
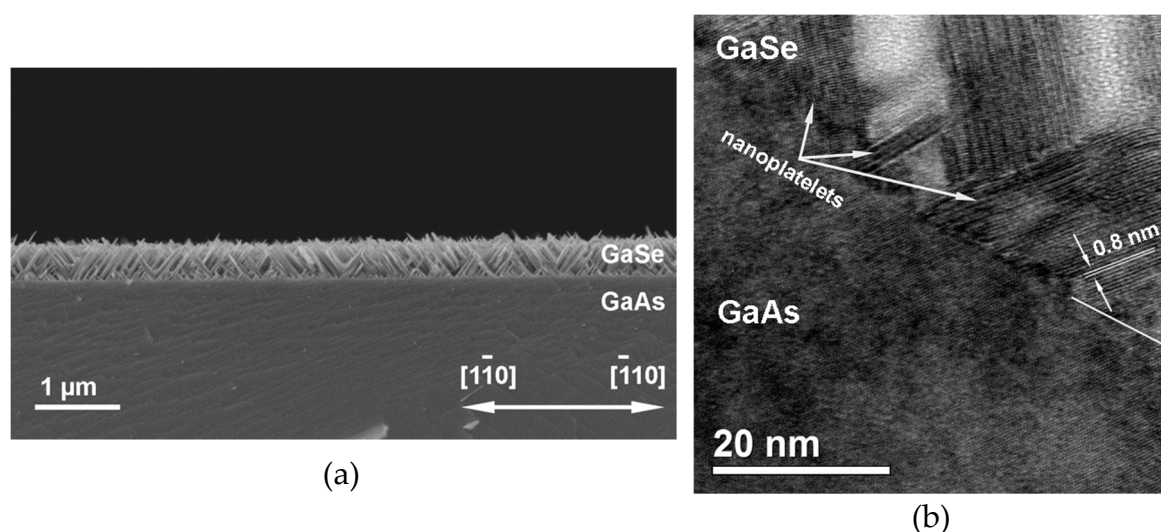

Figure 4. Cross-section SEM (**a**) and HRTEM (**b**) images of the GaSe layer grown on a GaAs(001) substrate at $T_S \sim 500\,°C$ (Se/Ga (BEP) ~ 25) (sample #*GS7*).

The X-ray powder diffraction patterns of the studied GaSe/GaAs(001) layers are presented in Figure 5. XRD patterns in addition to the reflections from the (002) and (004) planes of GaAs substrate demonstrate the reflections from GaSe planes oriented perpendicular to the *c* axis, which indicates the preferential orientation of the *c* axis in the direction normal to the growth surface. A weak additional peak in the angle range ~28.4° along the 2θ axis on XRD patterns of the layers grown under strong Se-rich conditions (Curves 1 and 2), can be attributed to the inclusions of a Ga_2Se_3 phase [30], since its position is in good agreement with the Ga_2Se_3(111) reflection [62], and the intensity is higher for the layer grown at the higher Se/Ga flux ratio. The preferred orientation of the Ga_2Se_3 phase is due to the proximity of interatomic distances in the GaSe(0001) and Ga_2Se_3(111) planes (i.e., along GaSe⟨1000⟩ and Ga_2Se_3⟨110⟩ directions), being 3.755 and 3.83 Å, respectively. According to Afifi et al. [62], the lattice constant of cubic α-Ga_2Se_3, determined from the analysis of the XRD patterns, is a = 5.44 Å. The existence of the Ga_2Se_3 phase inclusions in the GaSe layers grown under strong Se-rich conditions was also confirmed directly by TEM (Figure S3b).

In contrast to that, XRD patterns of the samples grown at nearly stoichiometric conditions (Curves 3–5 in Figure 5) demonstrate the absence of the Ga_2Se_3 peak. The XRD patterns of the GaSe layers, which possess rough surface morphology (Curves 3 and 5 in Figure 5), contain additional peaks that can be interpreted as reflections from the inclined GaSe planes. The appearance of these additional peaks in the X-ray diffraction pattern probably evidences the internal ordering or, in other words, indicates the existence of preferred tilt angles of the nanoplatelets.

The GaSe layers were studied also by Raman spectroscopy techniques. Figure 6 shows the Raman spectrum of the bulk ε-GaSe sample produced by HQ Graphene (Groningen, the Netherlands) (the bottom curve), which was measured in a scattering configuration with the incident light directed along the *c* axis, as well as the typical Raman spectra of the GaSe/GaAs(001) epilayers grown at different conditions. The Raman spectra were measured under 532 nm laser excitation. It can be seen that, in the spectra of all samples, in addition to the lines corresponding to vibrational modes in GaSe [63], there are two extra lines at frequencies of 268 and 291 cm^{-1}, which are associated with light scattering by transverse (TO) and longitudinal (LO) phonons in the GaAs substrate. However, in contrast to the spectrum of bulk ε-GaSe containing only one line near 213 cm^{-1}, a distinct doublet is observed in this spectral region in the spectra of the GaSe layers grown at $T_S \sim 500\,°C$ (Curves 4 and 5), as well as in the spectrum of the GaSe layer with the rough surface morphology grown at $T_S \sim 400\,°C$ (Curve 3,

#*GS8*). According to the selection rules [63,64], the line in the doublet, which we interpret as E″ mode, should appear in the spectrum, provided that the incident light is not directed strictly along the *c* axis. Thus, the presence of such a doublet is an indication of the substantial deviation of the *c* axis in the GaSe nanoplatelets from the normal to the substrate/layer interface. In addition, a broad peak with a frequency of about 250 cm^{-1} is observed in the spectra of the same samples. There are several explanations for its origin. This peak can be an E′(LO) mode from ε-GaSe, which manifests itself in the spectra as a result of the deviation of the *c* axis in the GaSe nanoplatelets from the normal to the substrate/layer interface, or it can arise due to symmetry breaking caused by imperfection of the crystal lattice [65,66]. On the other hand, this peak can also be associated with amorphous Se, which can exist on the surface, since GaSe is easily oxidized [32,67]. Thus, the obtained Raman data presented by Curves 3–5 in Figure 6 allow us to conclude that these layers predominantly possess an ε-GaSe polytype. The SAED measurements of the sample #*GS3* agree well with this assumption, indicating the hexagonal crystal structure of the grown layer. An additional argument in favor of this interpretation is the first-principle calculations which predict the ε-polytype being a more stable form in comparison with that of β-polytype also having a hexagonal crystal structure [65,68].
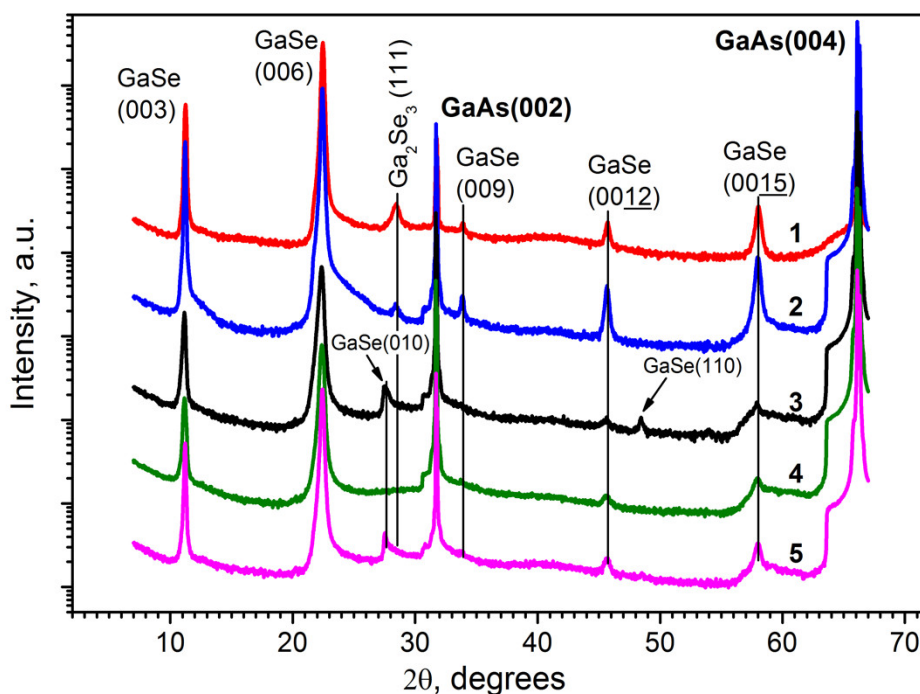

Figure 5. The X-ray powder diffraction patterns of the GaSe layers grown on GaAs(001) substrates. A weak additional peak in the angle range ~28.4°, along the 2θ axis on XRD patterns of the layers grown under strong Se-rich conditions at T_S = 400 °C (Curves 1 and 2), is attributed to the inclusions of a Ga$_2$Se$_3$ phase. Curves 1–5 correspond to samples #*GS2*, #*GS1*, #*GS5*, #*GS4*, and #*GS3*, respectively.

Curve 2 in Figure 6 shows the typical Raman spectra of flat GaSe layers grown at T_S ~ 400 °C under strong Se-rich conditions (sample #*GS1*). One can see that the fundamental difference between this spectrum and the spectrum of bulk ε-GaSe is the absence of a line at a frequency of 19 cm^{-1}. According to the group-theory analysis, the lowest frequency line in the Raman spectrum of GaSe should correspond to interlayer vibrations, and therefore should not be observed in the first-order Raman spectra of γ-GaSe because the primitive unit cell of γ-GaSe contains only one layer per unit cell [69]. Another peculiarity of Curve 2 in Figure 6 is that two lines in the spectrum are shifted to low frequencies compared to similar lines in the spectrum of bulk ε-GaSe, which are located at frequencies of 134 and 214 cm^{-1} (see also Figure S5). A similar shift of the lines was reported also by Yuan et al. [19], where the correspondence of the grown layer to the γ-GaSe polytype was determined using TEM.

An analysis of the Raman data for both ε- and γ-polytypes of GaSe presented by Hoff et al. [64] also leads to the conclusion that the low-frequency shift of the two phonon modes is a characteristic of the γ-GaSe polytype. Thus, the peculiarities in the Raman spectrum of the GaSe layer grown at $T_S \sim 400$ °C (Curve 2 in Figure 6) confirm the conclusion drawn earlier from SAED (Figure S3a) that sample #*GS1* is the γ-GaSe polytype. Summarizing, from the analysis of the Raman spectra of GaSe samples, we can conclude that the formation of a particular GaSe-polytype is determined not only by the epitaxial growth temperature, but rather by a combination of several factors.
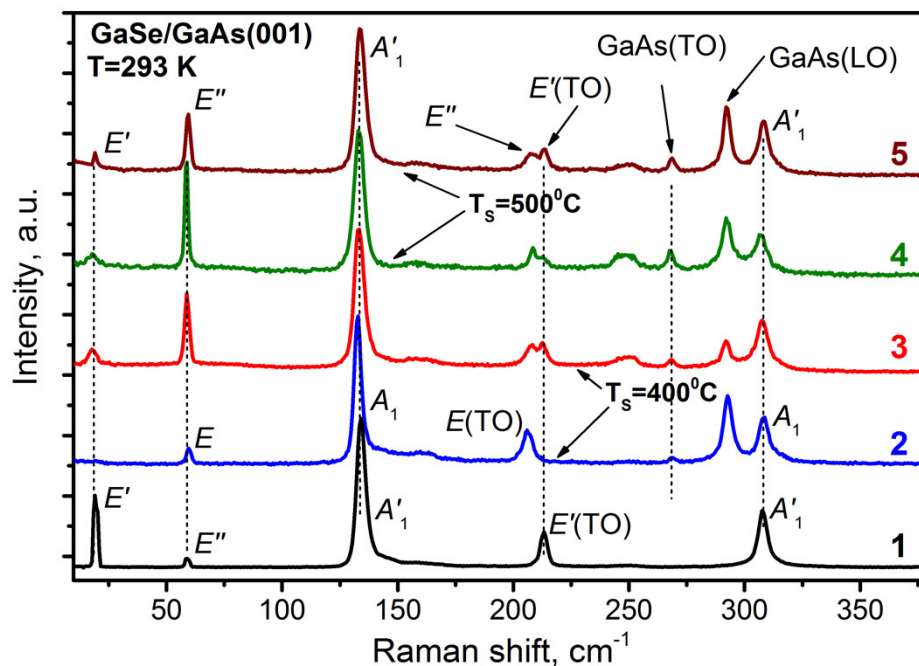
Figure 6. Raman spectrum of the bulk ε-GaSe layer produced by HQ Graphene (Curve 1). Raman spectra of the GaSe layers grown on GaAs(001) substrates at $T_S \sim 400$ °C (Curves 2 and 3, samples #*GS1* and #*GS8*, respectively), at $T_S \sim 500$ °C (Curve 5, sample #*GS7*), and using a two-stage growth mode (Curve 4, sample #*GS3*). All spectra are normalized to the intensity of the A_1 phonon line (132 cm^{-1}).

Figure 7a demonstrates the temperature-dependent PL spectra of the γ-polytype GaSe layer grown at $T_S = 410$ °C in Se-rich regime (sample #GS1). As can be seen in the figure, PL spectra at different temperatures demonstrate broad emission bands centered at around 1.7 eV. The peak near 1.5 eV is attributed to the emission from GaAs substrate. The main peak at 1.7 eV apparently consists of at least two peaks and its intensity rapidly quenches with increasing temperature. The observed PL spectra are very similar to those reported by Diep et al. for the GaSe/GaAs(001) layers also grown at $T_S = 400$ °C [55], where the PL peaks were attributed to the free and bound excitons, respectively, and the strong redshift in PL was explained by the strain-induced reduction of the GaSe bandgap energy due to the SDD growth mode. The MBE growth conditions of the GaSe layers in [55] are similar to those used for growing sample #*GS1* (see Table 1), where the occurrence of SDD growth mode is definitely highly likely due to the high Se/Ga ratio. However, when tensile strain is applied a noticeable shift of both A_1 compressional modes corresponding to the stretching vibrations of the atoms and located at frequencies of 134 cm^{-1} and 307 cm^{-1} should be observed [70,71]. Nevertheless, one can see no significant shift of the 307 cm^{-1} line in comparison with that of the bulk sample (Curves 1 and 2 in Figure 6). In addition, the observed rapid decay of the PL intensity with temperature allowed assuming the defect-related nature of this PL band. This assumption is supported by the fact that an intense emission band centered at 1.71 eV (77 K) was observed by Capozzi and Montagna [72] in the PL spectra of "poor-quality" GaSe samples grown from the melt by using the Bridgman–Stockbarger method. For each temperature studied, this emission band was more intense and broader in the

samples containing a higher density of structural defects or impurities with respect to the samples of good quality. Capozzi and Montagna proposed that this band originates from the recombination of free electrons, mainly at the indirect minimum, with neutral-acceptor levels [72]. A similar PL emission band was also observed in the PL spectra of GaSe/GaAs(001) layers grown at high $T_S > 500$ °C [49,73]. To make a reliable conclusion about the origin of the 1.7 eV peak in the PL spectrum of our GaSe layer #*GS1*, time-resolved PL measurements should definitely be carried out.
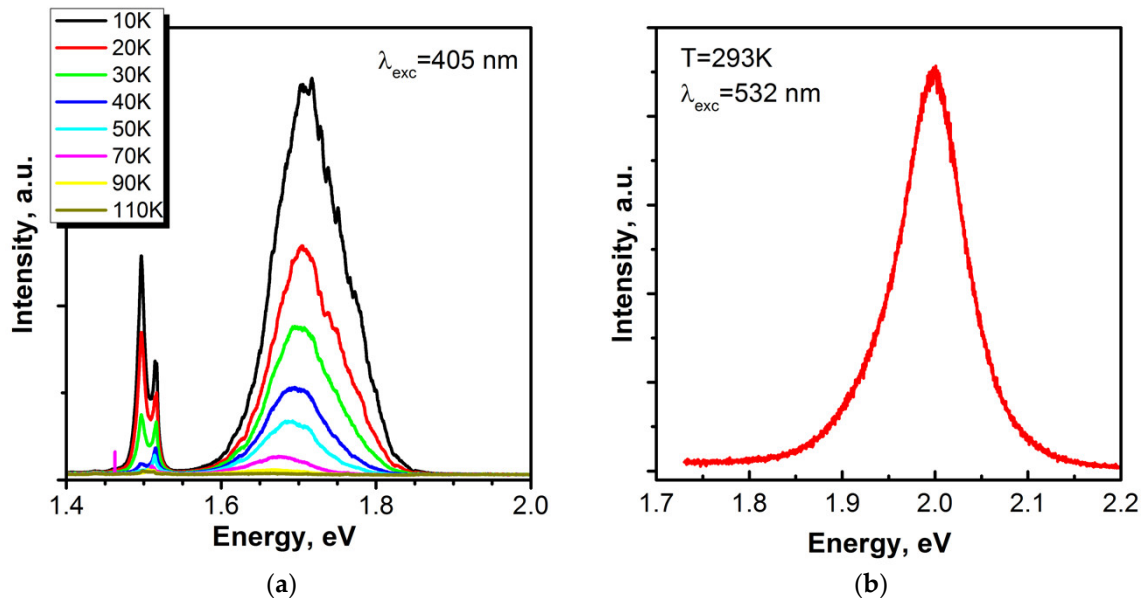
Figure 7. (**a**) μ-PL spectra of the GaSe layer grown at $T_S = 400$ °C as a function of temperature (sample #*GS1*). The laser power density on the sample was below 1 W/cm^2. (**b**) PL spectrum of the GaSe layer grown at $T_S = 500$ °C (sample #*GS7*).

In contrast to that, the GaSe layer grown at high $T_S \sim 500$ °C (sample #*GS7*) demonstrates strong PL at $T = 300$ K (Figure 7b). The spectral position (1.99 eV) of the emission line corresponds well to the emission line of the direct free exciton at $T = 300$ K [74]. The strong anisotropic dependence of the PL intensity (the details can be found in [75]) is evidence of a strictly oriented array of GaSe nanoplatelets in this structure, which is in a good agreement with TEM data.

3.2. MBE Growth of InSe-Based Heterostructures on GaAs(001) Substrates

The main problem in the MBE growth of InSe layers is associated with the formation of numerous In_xSe_y-type phases [36,76]. The relation between the film components and Se/In flux ratio corresponds to that appearing in the phase diagram [36]. In other words, one can expect the coexistence of In_4Se_3 with the main InSe phase at low Se/In flux ratios, as well as the occurrence of In droplets on the growth surface, while at high Se/In flux ratios the In_2Se_3 phase will predominantly crystallize. Indeed, the existence of "parasitic" In_xSe_y phases (mainly In_4Se_3) has been reported in the InSe layers grown in a wide range of growth conditions on different substrates: glass, Si(001), Si(111), GaAs(111), and GaAs(001) [22,73,77–80]. The most comprehensive study of the film composition as a function of both Se/In flux ratio and T_S was performed by Emery et al. for the InSe films grown by MBE on amorphous substrates using standard elemental In and Se effusion cells [22,79]. Chatillon et al. explained the experimental results by performing a thorough thermodynamic analysis of MBE growth in the In-Se system [76,81]. The difference between calculated and experimental impinging molecular fluxes was taken into account by introducing the Se incorporation coefficient, which is the usual way for the thermodynamic description of the MBE growth of Se-based semiconductors [82,83]. According to Brahim-Otsmane et al. [79], at the substrate temperature of $T_S \sim 350$ °C for Se/In BEP ratio R < 2, which corresponds to the nearly stoichiometric ratio between the adsorbed In and Se

adatoms on the growth surface [81], mixed films consisting of InSe and In_4Se_3 phases are grown, while at R > 3 the grown film is composed of InSe and γ-In_2Se_3 phases. Moreover, the relatively narrow "MBE growth window" for InSe films (R = 2–3) becomes narrower with increasing growth temperature up to T_S ~ 450 °C, and the In_4Se_3 phase inclusions are observed even in InSe layers grown at nearly stoichiometric conditions [79,84]. The formation of In_4Se_3 phase was also observed during the growth of InSe layers on GaAs(001) substrates, as confirmed by Raman measurements [75].

The growing of InSe films by using a Se valve cracking cell is even more complicated task. It should be noted that Ga_2Se_3 phase inclusions were observed in GaSe/GaAs(001) layers grown at a high cracking zone temperature ($T_{Se}(cr) = 950$ °C) of the Se valve cell even at nearly stoichiometric conditions [30]. In this case, the growth window for "pure" InSe becomes even narrower or, possibly, disappears completely, especially at high T_S. The Se/In BEP ratio corresponding to the nearly stoichiometric conditions is also changed by virtue of a change in the Se sticking coefficient.

In our experiments on MBE growth of InSe/GaAs(001) layers, the standard In cell and Se valve cracking cell with a cracking zone temperature of $T_{Se}(cr) = 500$ °C were used as molecular beam sources. The In beam flux was ~1.3×10^{-7} Torr (BEP), which corresponds to an average InSe growth rate of 1.2–1.3 nm/min. The layers were grown at $T_S = 450$ °C. This temperature was chosen to provide the maximum structural quality of growing film and simultaneously avoid the film re-evaporation. Suggesting the similar dependence of stoichiometric VI/III flux ratio on Se cracking zone temperature as in the case of GaSe, the nearly stoichiometric InSe/GaAs(001) MBE growth conditions at $T_S = 450$ °C were estimated as Se/In(BEP) ~5–6 ($T_{Se}(cr)$ ~ 500 °C). The InSe growth on GaAs(001) was initiated by the simultaneous opening of In and Se shutters.

The plan-view and cross-section SEM images of the InSe film grown directly on GaAs(001) substrate at $T_S = 450$ °C at nearly stoichiometric Se/In flux ratio are presented in Figure 8. One can see the film (hereinafter, sample *#IS1*) consists of a number of randomly oriented nanocrystallites, which confirms the difficulties in InSe nucleation on the GaAs(001) surface at high temperatures [73]. The different shape of the nanocrystallites may also indicate the presence of secondary phase inclusions.
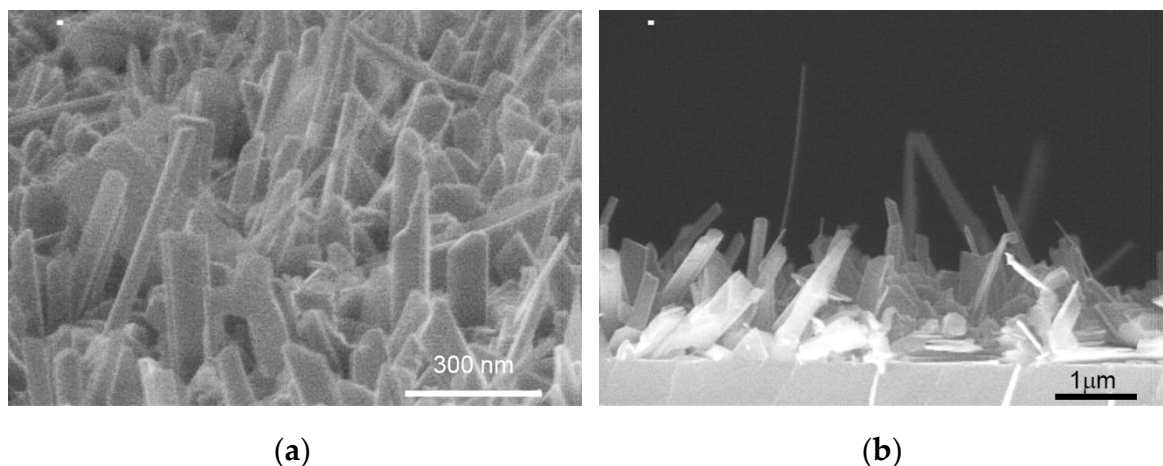

(a)   **(b)**

Figure 8. The plan-view (**a**) and cross-section (**b**) SEM images of the InSe/GaAs(001) film (sample *#IS1*) grown at $T_S = 450$ °C at nearly stoichiometric growth conditions.

The X-ray powder diffraction pattern of the InSe/GaAs(001) layer (sample *#IS1*) is presented in Figure 9. The most intense diffraction peaks are attributed to InSe (00l), which indicates that there are a lot of InSe crystallites whose **c** axis is perpendicular to the substrate plane. The significant part of additional peaks can be attributed as belonging to the In_4Se_3 phase [84,85], and the intensities of these peaks (marked by black circles) are comparable with that from InSe. We assume that the presence of a significant amount of the In_4Se_3 phase in the film is associated primarily with the MBE growth conditions used, but also with the use a valve cracking cell as a Se source. Due to the similar positions

of (003n) and (002n) reflections in the XRD pattern of rhombohedral and hexagonal InSe crystals, it is difficult to conclude which InSe polytype occurs. The intense peak at 2θ = 29.00 can be an indication of rhombohedral symmetry, since reflection at this Bragg angle exists only in powder XRD of the rhombohedral InSe modification [86]. However, this peak can also be associated with (040) reflection of In_4Se_3. The existence of additional asymmetric reflections on XRD pattern agrees well with observed surface morphology of the film.

The InSe reflections in Figure 9 are indexed for the γ-InSe rhombohedral lattice, since in this case the positions of asymmetric peaks are found to fit better the measured XRD pattern; we used the lattice parameters of rhombohedral InSe reported by Nagpal and Ali [42]: a = 4.0046 Å and c = 24.960 Å.
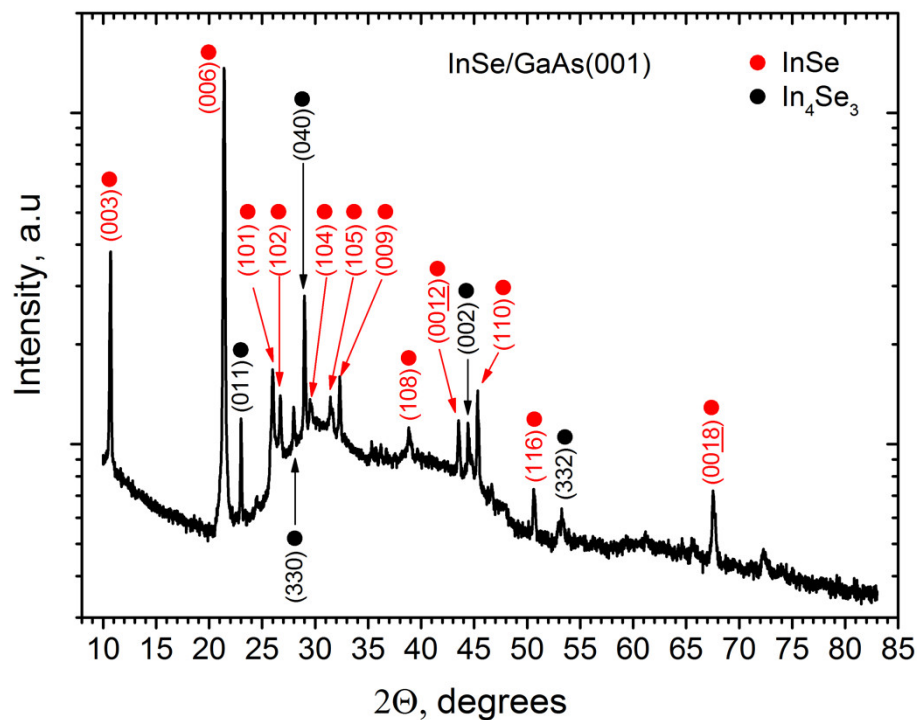

Figure 9. The X-ray powder diffraction pattern of the InSe/GaAs(001) layer (sample *#IS1*). Reflections corresponding to InSe are indicated by red circles, while reflections that can be attributed to the In_4Se_3 phase are marked by black circles. The InSe reflections are indexed for the γ-InSe rhombohedral lattice.

Raman spectra of the InSe/GaAs(001) layer (sample *#IS1*) measured at 80 and 300 K are shown in Figure 10. The line at 532 nm of Nd:YAG laser was used as the excitation source. Five peaks located at 18, 41, 115, 177, and 227 cm^{-1} are clearly seen in the room temperature Raman spectrum. These values are typical for InSe phonon modes measured under off-resonance conditions [87]. The phonon frequencies increase by a few cm^{-1} with decreasing temperature from 300 to 80 K. Additional peaks in the low temperature Raman spectrum detected at 38, 72, 104, and 168 cm^{-1} can be associated with the presence of In_4Se_3 phase [73,84], which is in a good agreement with XRD measurements. As mentioned above, according to XRD data, the InSe/GaAs(001) layer has a rhombohedral lattice, which indicates a γ-InSe polytype. However, the presence in the Raman spectrum of a low-frequency line at 18 cm^{-1} is in contradiction with this statement. According to the group-theory analysis, the lowest frequency line in the Raman scattering spectrum of InSe should correspond to interlayer vibrations [88]. The primitive unit cell of γ-InSe contains only one layer per unit cell and therefore this line should not be observed in the first-order Raman spectra. The appearance of this line is an important signature of presence of either ε- or β-phase InSe [87]. On the other hand, in the Raman spectra of non-centrosymmetric γ- and ε-InSe polytypes, polar longitudinal (LO) modes should be observed in certain scattering geometries and the intensity of those modes is enhanced in resonance conditions [89–91].
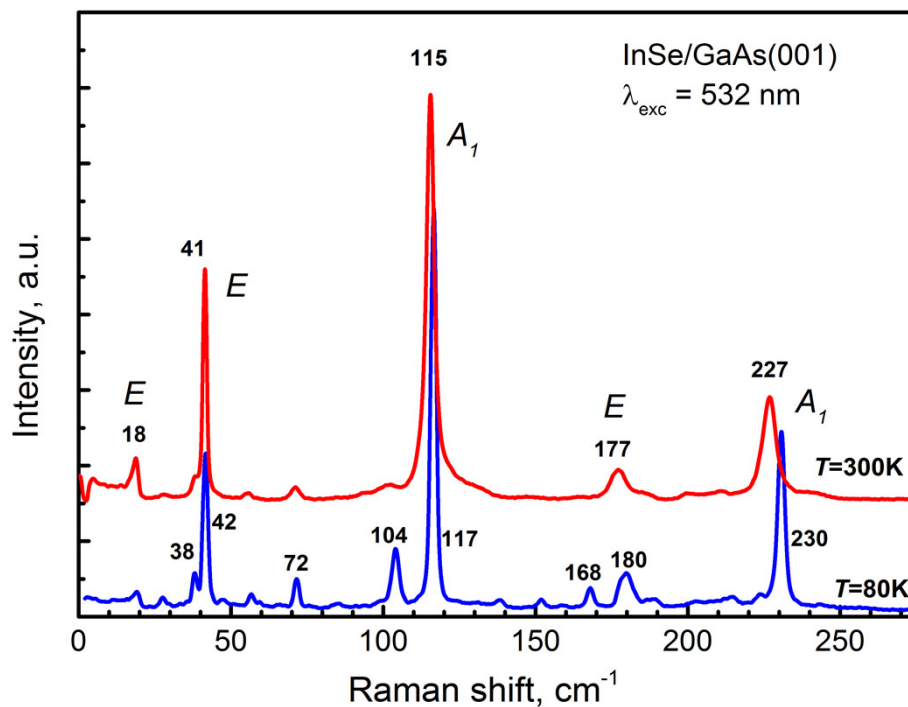
Figure 10. The Raman spectra of the InSe/GaAs(001) layer (sample #*IS1*) measured at 300 K (red curve) and at 80 K (blue curve). The symmetrycep of the phonon modes are given in accordance with [87].

To clarify the reason for the contradiction between the XRD and Raman data, the measurements were made in the near-resonance Raman scattering using 514.5 and 488 nm lines of Argon laser as excitation sources. For γ-InSe, the 514.5 nm line has energy of about 10 meV below the E_1' exciton energy, while the energy of the 488 line is 9 meV above the exciton energy at the respective temperatures [91]. The corresponding spectra are shown in Figure 11 together with the off-resonance Raman spectrum obtained using the line at 532 nm as an excitation source. It can be seen that at room temperature a new doublet feature with frequencies of 199 cm^{-1} and 211 cm^{-1} is observed upon excitation at 514.5 nm. In the spectrum at T = 80 K obtained upon 488 nm excitation, the doublet feature experiences a high-frequency shift and a significant increase in intensity. Similar spectra for γ-rich bulk InSe were reported for the first time by Kuroda and Nishina [91]. It should be noted that in this work, upon excitation by the 514.5 and 488 nm lines, a low-frequency line was detected in the region of about 17–18 cm^{-1} in the Raman spectra (similar to that shown in Figure 11). However, this line, as already discussed above, should not be observed for the pure γ-InSe.

The spectra shown in Figure 11 make it possible to exclude the presence of β-phase in the InSe/GaAs(001) layer, since polar (LO) phonon modes that could be resonantly enhanced are absent in the Raman spectrum of β-InSe polytype [90]. Thus, taking into account the XRD data, the InSe/GaAs(001) layer (sample #*IS1*) can be characterized as γ-rich InSe, implying that along with the main γ-phase of InSe there exists also a certain amount of ε-phase. This result is in good agreement with the fact that MBE grown InSe films are usually of γ-polytype [73,78,80,92,93].

The PL spectra of the InSe/GaAs(001) layer (sample #*IS1*) measured within the temperature range of 11–110 K are presented in Figure 12. A 405 nm violet diode laser SSP-DHS-405 was used as the excitation source; the excitation power was as low as 50 mW, which corresponds to the excitation power density of ~0.5 W/cm^2. The highest-energy peak observed in the PL spectrum at T = 11 K is detected at ~1.307 eV. This is more than 30 meV lower than the exciton recombination line (1.338 eV) recently reported by Shubina et al. [94] for flakes freshly cleaved from high structural quality bulk InSe grown by the Bridgman–Stockbarger method. According to the previous results [95,96], in the region below 1.32 eV, three main broad bands around 1.31, 1.28, and 1.23 eV have been reported in undoped InSe, which were assigned to impurity-band, donor–acceptor pair, and impurity-vacancy complex

transitions, respectively. In a good agreement with these reports, the low-temperature spectrum shown in Figure 12 (at T = 11 K) can be also approximated by at least three different Gaussian peaks centered at 1.307, 1.28, and 1.23 eV, respectively. The broad peak at 1.307 eV (T = 11 K), which dominates the spectrum at low temperatures, quenches quickly with increasing temperature and disappears at T ≈ 50 K. At temperatures higher than 40 K, the defect-related band begins to dominate in the spectra. However, at temperatures higher than 60 K, one can see an occurrence of a clearly resolved peak centered at ~1.314 eV. From the PL temperature dependence, we can assume that the initial broad peak centered at ~1.307 eV (T = 11 K) actually consists of two closely spaced peaks located at 1.301 and 1.315 eV. Indeed, the spectrum at T = 11 K is most accurately approximated by four Gaussian contours (Figure S6). Homs and Marí [97] performed a comparative study of the PL of undoped and slightly neutron-transmutation doped InSe samples. In the region around 1.31 eV in doped samples, they found two closely-spaced and poorly separated bands, which they indexed as *E* and *F*, respectively. These bands correspond well to *P1* and *P2* peaks in Figure S6. They found also that emission *F* thermally quenches faster than *E*. The peak *E* was attributed to the recombination of a native acceptor, while peak *F* was assigned to donor–acceptor pair transition where both donors and acceptors are ionized. Indeed, in our case, we observe a similar temperature dependence of *P1* and *P2* peaks (see Figure 12a) and, accordingly, we can accept the proposed interpretation. In the same way, the band at 1.28 eV also can be attributed to a donor–acceptor pair transition [96,97] due to its fast temperature quenching. Thus, these three transitions (*P1*, *P2*, and *P3*) could be assigned to InSe native impurities (defects) because they have been observed in undoped samples [97]. Finally, the broad band observed at ~1.23 eV at T = 11 K can be associated with structural defects in the crystal. The presence of this band is an indication of a high concentration of defects and this band is assigned to a transition within an impurity vacancy-complex [95,96].
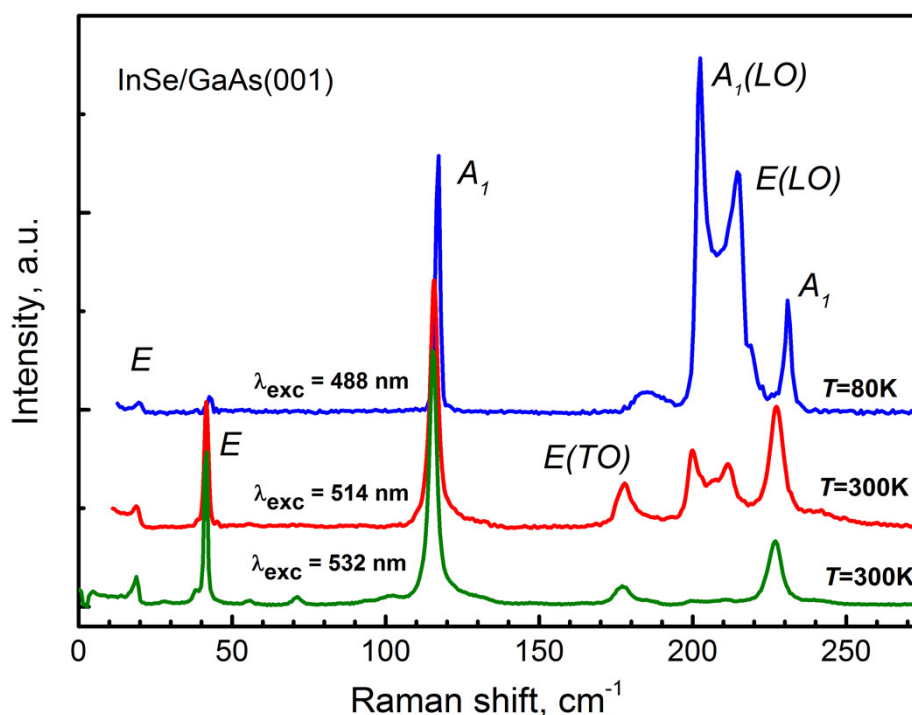

Figure 11. The near-resonance Raman spectra of the InSe/GaAs(001) layer (sample #*IS1*) measured at 300 K (λ_{exc} = 514.5 nm, red curve) and at 80 K (λ_{exc} = 488 nm, blue curve) along with the off-resonance Raman spectrum of the same layer measured at 300 K (λ_{exc} = 532 nm, green curve). The spectra are normalized to the intensity of the A_1 (115 cm^{-1}) phonon line.
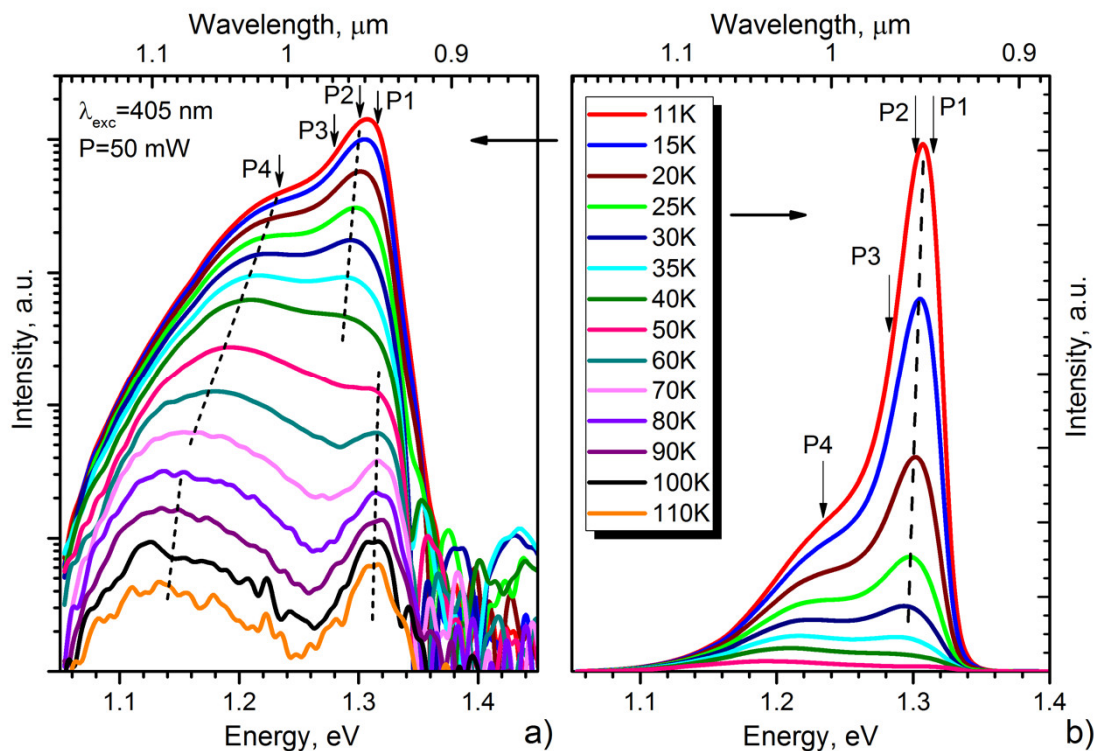
Figure 12. Photoluminescence spectra of the InSe/GaAs(001) layer (sample *#IS1*) at a low excitation power of 0.5 W/cm^2 in logarithmic (**a**) and linear (**b**) scales measured at different temperatures. The colors of the curves correspond to the legend presented in (**b**). The *P1*, *P2*, *P3* and *P4* peaks correspond to those shown in Figure S6. The dashed lines are shown for eyes only and correspond to temperature shift of the respective peak maxima.

To improve the surface morphology of the layer, it is apparently possible to use the two-stage growth technique, which involves the deposition of the InSe buffer layer at low T_S in order to form a more planar interface [98,99]. A more advanced strategy involves the use of a GaSe buffer layer [73,80]. To control the film orientation, Budiman et al. also used the GaAs(001) substrates misoriented by 2° or 5° toward [110] direction [73]. However, despite the relatively planar surface morphology of the GaSe buffer layer (see Section 3.1), the top InSe layer grown at high T_S ~ 450 °C is again composed of a number of microcrystallites (see Figure S7). The observation of Debye rings in the RHEED pattern during MBE growth of InSe also confirms the polycrystalline nature of the film.

The strong diffusion of Ga into the top InSe layer with the formation of the InGaSe alloy was observed in the InSe/GaSe/GaAs(001) heterostructure, where the InSe growth temperature was as high as $T_S \approx 465$ °C. The RT Raman spectrum of this structure is presented in Figure 13 (upper curve) along with the Raman spectra of reference InSe/GaAs(001) (middle curve) and γ-GaSe/GaAs(001) (lower curve) layers. The Ga diffusion into the top InSe layer is confirmed by the shift of all InSe Raman peaks in comparison with the reference InSe/GaAs(001) layer. The weak peaks at 59 and 132 cm^{-1} in the upper curve in Figure 13 correspond to the underlying GaSe buffer layer. It should be noted that strong interdiffusion at the InSe/GaSe interface at the growth temperatures of InSe higher than 400 °C was observed also in previous works [73,80].

Taking account of difficulties in InSe/GaAs(001) heteroepitaxy, as well as the problems with high-temperature InSe growth on GaSe surface, we tried to realize the ZnSe/InSe/ZnSe quantum well (QW) heterostructures. The InSe/ZnSe looks as a promising heteropair for potential applications in the field of photonics and electronics, when taking into account the fact that the band line-up for the InSe/ZnSe interface was reported to be of strong type I [100] as well as the existence of matured MBE technology of ZnSe/GaAs(001) [59].
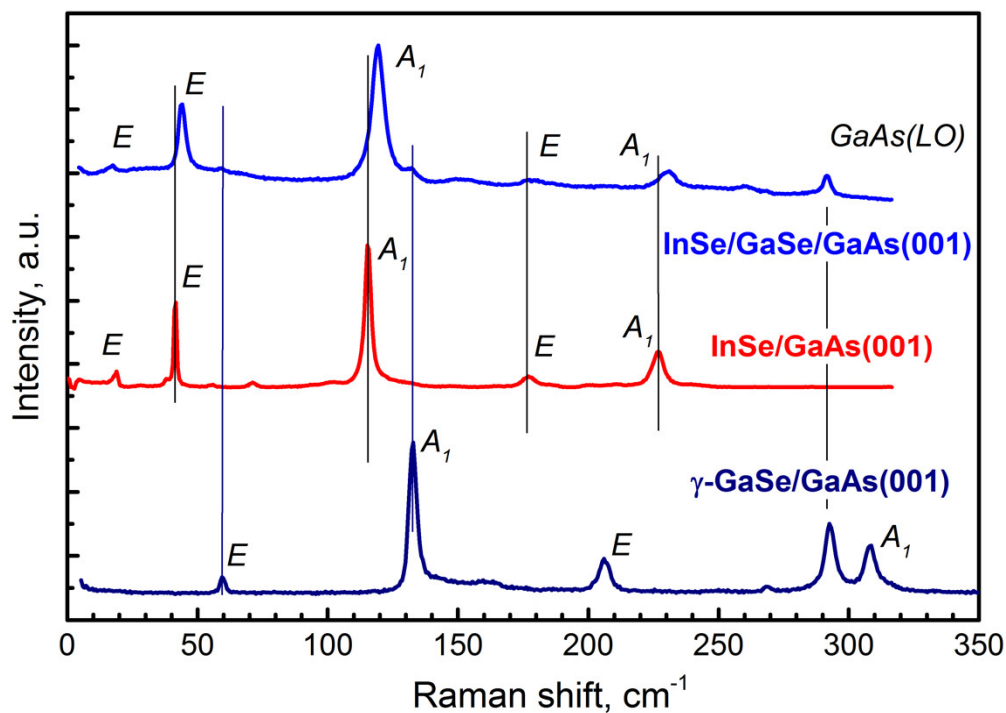
Figure 13. The Raman spectrum (upper curve) of the InSe/GaSe/GaAs(001) structure along with the Raman spectra of both InSe/GaAs(001) (sample #*IS1*, middle curve) and γ-GaSe/GaAs(001) (sample #*GS1*, lower curve) layers (T = 300 K). The spectra are normalized to the intensity of the A_1 (115 cm^{-1}) phonon line.

The nominal thickness of InSe layer in the ZnSe/InSe/ZnSe QW heterostructures ranged 2–7 TLs. The thicknesses of the ZnSe bottom and top layers were 80–160 and 20–40 nm, respectively. The growth conditions of InSe on ZnSe(001) surface were chosen the same as in the case of InSe/GaSe heteroepitaxy: T_S = 450 °C and flux ratio Se/In (BEP) ~ 5–6. The top ZnSe layer on the InSe surface was grown at T_S = 300 °C. The details of MBE growth of ZnSe/InSe/ZnSe QW heterostructures as well as studies of their surface morphology were recently reported by Avdienko et al. [101]. Here, we focus mainly on the structural and optical properties of these QW structures.

Figure 14a shows the cross-sectional high-resolution TEM image of the ZnSe/InSe/ZnSe QW structure with a 7-TL-thick InSe layer. The TEM data confirm the multi-domain character of InSe/ZnSe(001) nucleation. At the growth conditions used, the *c* axis of InSe is directed normal to the growth surface. The TEM data also confirm the (111)-oriented ZnSe growth on the InSe(0001) surface, as previously reported by Smathers et al. [102]. However, the orientation of the ZnSe layer remains unchanged in those parts of the structure where there are no InSe islands. The existence of the (111)-oriented ZnSe phase in the structure was also confirmed by SAED measurements [101]. We suppose that the growth of ZnSe with a (111) orientation onto the InSe(0001) van der Waals surface is caused by the proximity of the InSe and ZnSe(111) lattice parameters (Δa/a ~ 1% or less, a(InSe) = 4.005 Å [41]). Therefore, the InSe islands provide the epitaxial orientation of the upper ZnSe layer, despite the weak interaction between them. In this case, the island-like growth of ZnSe(111) can be explained in terms of minimizing the elastic energy of the growing layer [101].

All QW structures demonstrate similar PL independent from InSe nominal thickness. One can see the intense broad line centered at ~2.27 eV (Figure 14b), indicating the same origin of this line in all QW structures. The time-resolved PL measurements demonstrate that the PL decay time is large and also nearly the same (~270 ns) in all structures (Figure 14c). Therefore, we can assume the luminescence is associated with radiative recombination centers of In in ZnSe because of the In diffusion into the underlying ZnSe layer. This assumption agrees well with the experimental value of the acceptor level

energy in ZnSe crystals doped with indium, which is ~0.41 eV above the valence band [103]. A similar PL line at ~2.25 eV was also previously observed in In-doped ZnSe crystals [104].
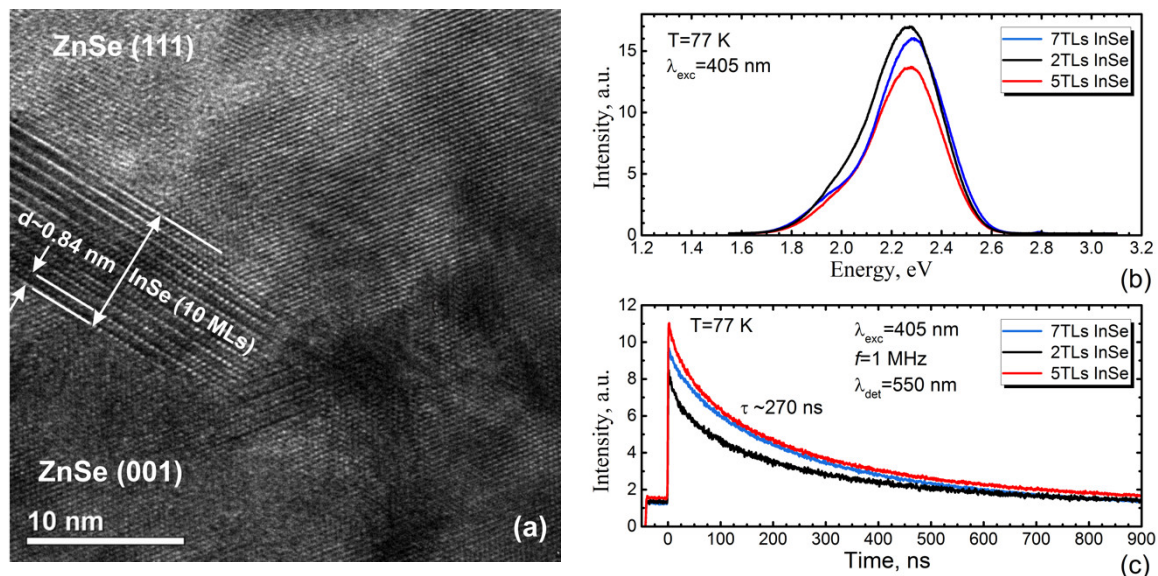

Figure 14. (**a**) Cross-section HRTEM image of the ZnSe/InSe/ZnSe QW structure with the InSe nominal thickness of ~7 TLs; (**b**) PL spectra of ZnSe/InSe/ZnSe QW structures with different InSe nominal thickness; (**c**) time-resolved measurements of the luminescence in ZnSe/InSe/ZnSe QW structures at T = 77 K. The samples were excited by 405 nm radiation of the CUBE laser (Coherent) with pulses of 45 ps duration at a repetition rate of 1 MHz.

3.3. MBE Growth of GaTe Layers and GaTe/GaSe Heterostructures on GaAs(001) Substrates

As mentioned above, one of the main problem in the MBE growth of different layered III-VI's is the formation of numerous "parasitic" phases, i.e., In_4Se_3 and In_2Se_3 [73,101] or Ga_2Se_3 [28,30] in the case of MBE growth of InSe and GaSe, respectively. For the Ga-Te system, the other possible stable phase is Ga_2Te_3 [105]. The Ga_2Te_3 films were successfully synthesized by metalorganic MBE on both InP(001) and GaAs(001) substrates at T_S = 400–500 °C under strong Te-rich conditions (Te/Ga ~ 30) [106,107]. However, no evidence of Ga_2Te_3 inclusions has been obtained in MBE grown GaTe/GaAs(001) epilayers at much lower (Te/Ga ~ 10) flux ratio [108].

In this study, GaTe layers were grown on GaAs(001) substrates via a 200-nm-thick GaAs buffer layer under Te-rich conditions at low $T_S \approx 450$ °C (sample #*GT1*) and high $T_S \approx 530$ °C (sample #*GT2*) substrate temperatures, respectively. The GaTe growth was initiated by the simultaneous opening of both Te and Ga fluxes onto the GaAs(001) surface. The Te/Ga flux ratios were chosen to provide the Te-rich conditions in accordance with Bae et al. [108]. The growth parameters as well as thicknesses of GaSe layers are outlined in Table 2.

Table 2. The growth parameters of GaTe/GaAs (001) layers.

Layer	T_{Ga}; Ga Flux (BEP)	Te/Ga Flux Ratio, (BEP)	T_S, °C	Layer Thickness, nm (SEM)	Average Growth Rate[2], nm/min	Notes
#*GT1*	900 °C; 4.0×10^{-8} Torr.	Te/Ga (BEP) ~ 11	450	230	1.28	0.2-μm-thick GaAs buffer layer
#*GT2*	920 °C; 6×10^{-8} Torr.	Te/Ga (BEP) ~ 15	530	200	1.82	0.2-μm-thick GaAs buffer layer

As mentioned above, GaTe preferentially crystallizes in the monoclinic α-structure (m-GaTe), which is more stable than the hexagonal close-packed β-structure (h-GaTe) [108–110]. The metastable phase h-GaTe generally exists in ultrathin samples [109,111]. However, under appropriate growth

conditions, thick hexagonal GaTe flakes can be also obtained. Yu et al. recently demonstrated the phase-controlled synthesis of monoclinic and hexagonal GaTe using conventional physical vapor deposition technique [112]. They found that growth temperature is the key factor for phase control of GaTe flakes, and h-GaTe flakes are intended to be stable under relatively low deposition temperature. The importance of low deposition temperature for h-GaTe fabrication is also in a good agreement with the growth conditions reported for the GaTe films grown by metal-organic chemical vapor deposition [113]. According to reported results, h-GaTe is a thermodynamically unstable phase and converts into monoclinic one (m-GaTe) with the increase in sample thickness or environmental temperature [108,109,113]. In particular, the thickness-dependent transformation of h-GaTe to m-GaTe has been reported for the GaTe layers grown by MBE on GaAs(001) substrates [108]. At substrate temperature $T_S \approx 450$ °C and Te/Ga(BEP) = 10, the critical thickness of such transformation has been estimated as high as ~90 nm.

The growth temperature is the main factor affecting the properties of the III–VI layers. Generally, the layers grown at higher T_S demonstrate the better crystal and optical quality. The plan-view SEM images of the samples #GT1 and #GT2 grown at different T_S are presented in Figure 15. The surface morphology of sample #GT1 (Figure 15a) is typical for the MBE grown III–VI layers and is very similar to the surface morphology observed in the GaSe layers grown at low $T_S \sim 400$ °C (see Figure 2). In contrast, the plan-view SEM image of sample #GT2 (Figure 15b) exhibits pronounced surface relief anisotropy, which is either related to the strong anisotropic nature of the m-GaTe crystal structure or induced by the large lattice mismatch between the GaTe and GaAs(001) substrate.
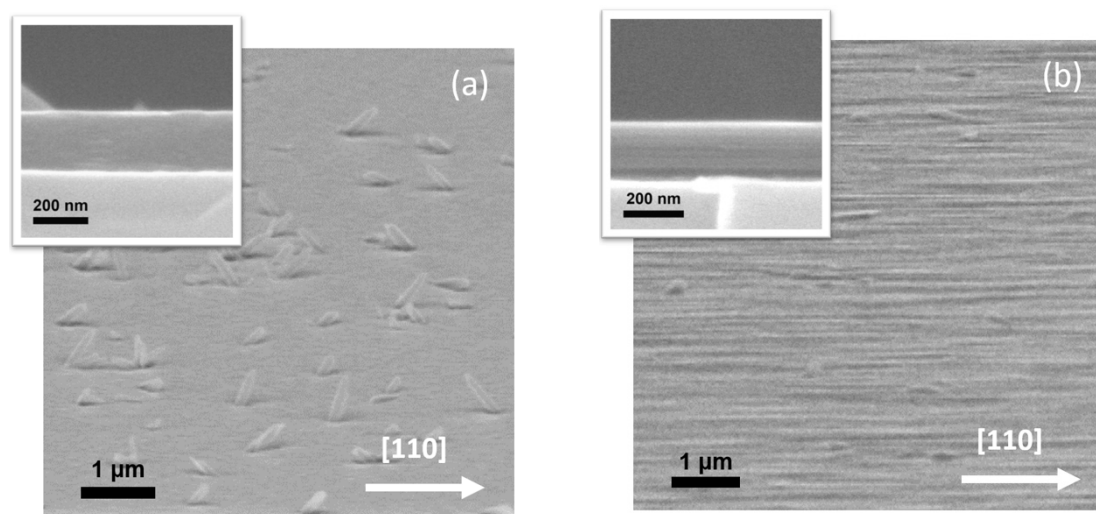

Figure 15. Plan-view SEM images of the GaTe layers grown on GaAs(001) substrates at different substrate temperature: (**a**) sample #GT1, $T_S \approx 450$ °C; (**b**) sample #GT2, $T_S \approx 530$ °C. The insets show the cross-section SEM images of corresponding structures.

An increase in the growth temperature can lead to chemical interaction between the substrate and the growing layer. This interaction in case of GaSe/GaAs(001) MBE growth ($T_S > 500$ °C) results in the significant surface morphology transformation because of the growth of inclined nanoplatelets (see Figure 4). However, the cross-section SEM image of GaTe layer (sample #GT2) (see inset in the Figure 15b) grown at high $T_S \approx 530$ °C demonstrates the formation of a relatively flat layer with nearly abrupt GaTe/GaAs(001) interface.

The RHEED images during the growth of samples #GT1 and #GT2 are presented in Figure 16. One can see that the RHEED patters remain streaky for both samples. However, the reflections for sample #GT1 grown at low temperature ($T_S \approx 450$ °C) are thickened and blurred (Figure 16a,b), and the brightness of the RHEED pattern gradually decreased with increasing the layer thickness. This behavior reflects an increase in the surface roughness as the layer grows, and can be induced by the formation

of multi-domain structure at the initial growth stage, i.e., the MBE growth of GaTe is similar to that observed for GaSe/GaAs(001) at low substrate temperatures. In contrast, the RHEED pattern of sample *#GT2* ($T_S \approx 530\ °C$) demonstrates much narrower streaky reflections (Figure 16c), confirming that the higher is the growth temperature, the higher is the crystal quality of the growing film.
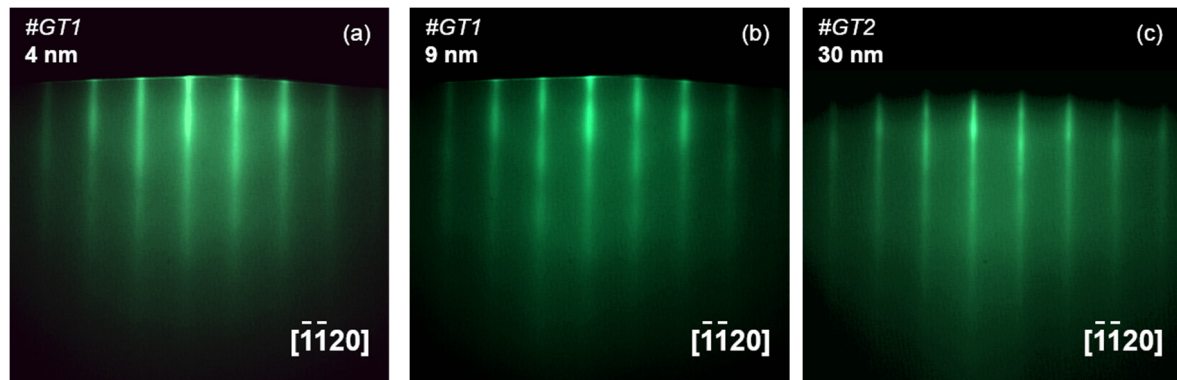

Figure 16. The evolution of the RHEED patterns along the $[1120]$ direction in MBE of GaTe/GaAs(001) epilayers grown at low $T_S \approx 450\ °C$ (sample *#GT1*): (**a**) the layer thickness of ~4 nm; (**b**) the layer thickness of ~ 9 nm; (**c**) the RHEED pattern of sample *#GT2* grown at $T_S \approx 530\ °C$ (the layer thickness is ~30 nm).

To understand the difference between samples *#GT1* and *#GT2*, we performed PL measurements. The as-grown samples were transferred through the air from MBE load-lock chamber into a closed-cycle helium cryostat. After that, they were stored in vacuum at room temperature for three weeks. The PL spectra were measured at T = 11 K in a closed-cycle helium cryostat using a laser source with the excitation wavelength of $\lambda_{exc} = 405$ nm. The laser power on the sample was as low as 50 mW with a spot of ~0.1 cm^2, which corresponds to the excitation power density of 0.5 W/cm^2. PL spectra of sample *#GT2*, measured after different storage times (within three weeks) are shown in Figure 17. The spectra are almost identical, confirming the absence of degradation of the GaTe optical properties during vacuum storage.
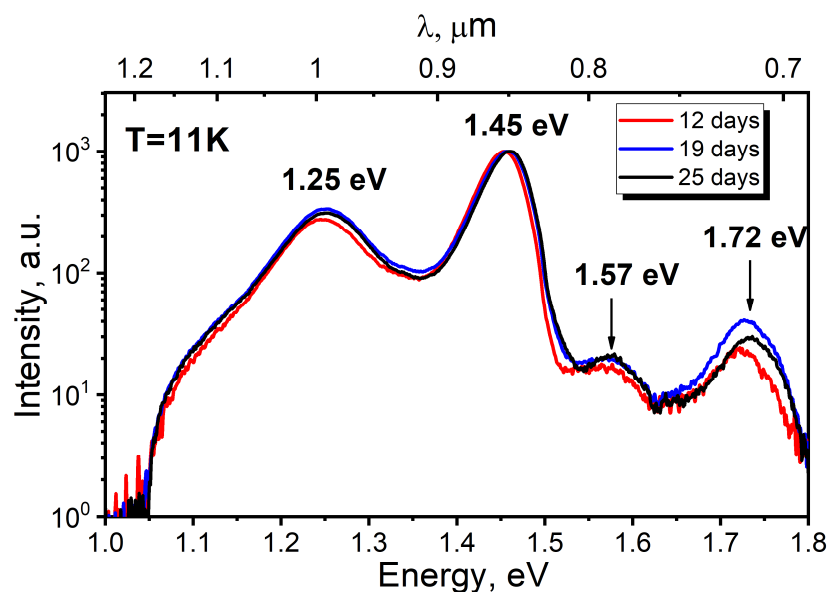

Figure 17. PL spectra of the GaTe/GaAs(001) layer *#GT2* measured after different storage time in vacuum (within three weeks). The PL intensity is normalized to the PL peak with energy of 1.45 eV.

The shortest wavelength peak located at ~1.72 eV could be associated with the emission of acceptor-bound excitons [114], while the broad band centered at 1.57 eV is presumably associated with donor–acceptor pair (DAP) recombination [115]. This interpretation is in good agreement with the assumption that Te-rich growth conditions should cause the GaTe layer to exhibit p-type natural conductivity [108]. One of the possible explanations of 1.45 eV peak is that it originates from the GaAs substrate. However, this peak was not observed in the PL spectrum of sample #*GT1*, and the PL maximum is shifted by ~50 meV toward a longer wavelength compared to the peak from the GaAs substrate. It is also highly unlikely that this peak is due to radiation from the hexagonal h-GaTe. Although the weak broad PL emission at 1.44 eV (T = 300 K) was observed by Fonseca et al. [116] from the hexagonal GaSe$_x$Te$_{1-x}$ islands with low Se content (x ≤ 0.05), according to Cai et al. [117], the hexagonal GaTe should possess the bandgap at 1.03 eV, which does not correlate with intense emission at 1.45 eV. Moreover, the X-ray powder diffraction pattern of sample #*GT2* (Figure 18a) indicates the dominance of monoclinic GaTe [108,110]. Cai et al. [118] argued that this peak is associated with the emission centers localized at the domain edges. The dominance of this emission band (1.45 eV) in our PL spectrum, measured at much lower excitation power density in comparison with that used by Cai et al., also supports this attribution. The absence of this peak in the sample #*GT1* grown at $T_S ≈ 450$ °C can be associated with much worse structural perfection of #*GT1* layer compared to #*GT2*. The peak at 1.25 eV, which is the only one registered in the PL spectra of both samples (#*GT1* and #*GT2*), probably corresponds to the radiation of a gallium vacancy complex in the GaAs substrate [119]. This assumption was confirmed by observation of the same peak in the PL spectrum of the bare GaAs substrate without the GaTe layer. Nevertheless, this peak can also be related to the defect emission in GaTe, since the PL intensity at 1.25 eV in sample #*GT2* is by an order of magnitude higher.
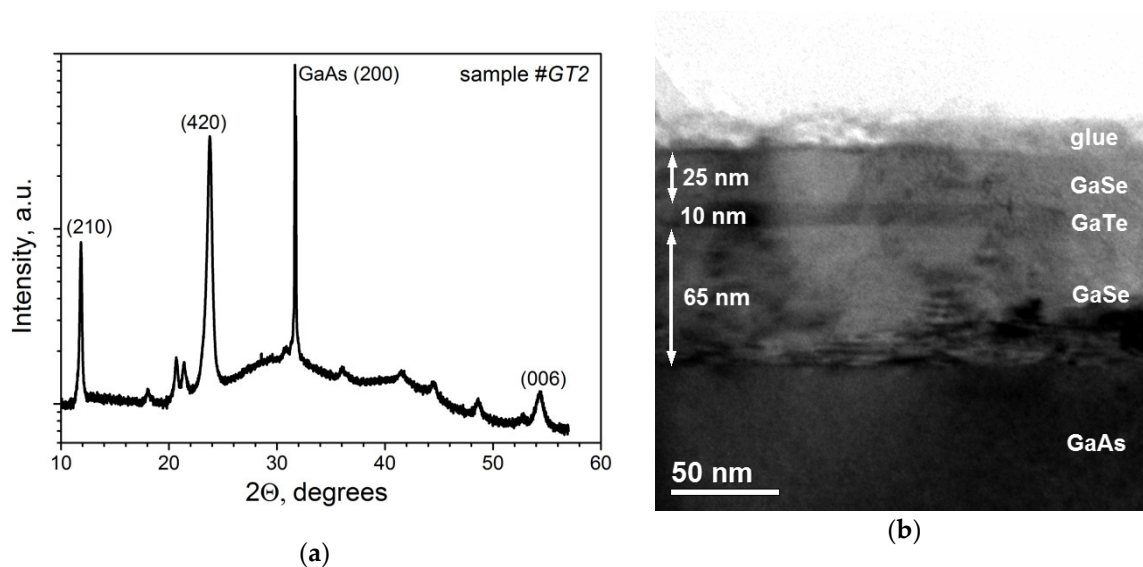

Figure 18. (**a**) The X-ray powder diffraction pattern of GaTe layer grown at $T_S ≈ 530$ °C (#*GT2*); (**b**) cross-section TEM image of the GaSe/GaTe/GaSe heterostructure.

The GaSe/GaTe system is perspective for the fabrication of QW structures due to a type I band alignment at GaSe/GaTe interface [120]. The GaSe/GaTe/GaSe heterostructure was grown on GaAs(001) substrate with a 200-nm-thick GaAs buffer layer. To provide the relatively flat growth surface for the GaTe deposition, the bottom GaSe layer was grown at relatively low $T_S = 400$ °C with Se/Ga(BEP) ~ 20 flux ratio. The average growth rate of GaSe was as low ~1.3 nm/min. GaTe layer was deposited at $T_S = 450$ °C, using the similar growth conditions as in sample #*GT1*. The growth temperature of the top GaSe was chosen also equal to $T_S = 400$ °C to avoid the Se diffusion into the GaTe layers. The TEM image of the GaSe/GaTe/GaSe heterostructure is presented in Figure 18b. It can be seen that the GaTe layer differs in contrast from GaSe and forms a rather uniform layer. The interfaces

between 2D materials are rather sharp. However, no PL has been revealed from the GaSe/GaTe/GaSe QW heterostructure. We assume that the main reason for the absence of PL in GaTe QW is a low growth temperature of both GaTe QW and GaSe barriers.

4. Conclusions

GaSe, InSe, and GaTe layers as well as the relevant heterostructures were grown by MBE on the GaAs(001) substrates at T_S = 400–530 °C using a standard Ga, In, and Te effusion cells as well as a Se valve cracking cell with the cracking zone temperature T_{Se}(cr) = 500 °C as molecular beam sources. The structures were studied in detail using SEM, TEM, X-ray diffraction, Raman, and PL spectroscopy techniques. The growth conditions corresponding to the stoichiometric ratio of Ga and Se adatoms on the growth surface as a function of growth temperature, as well as the correlation between the growth conditions and the properties of the GaSe layers were established. Powder X-ray diffraction has shown that the GaSe layers grown under strong Se-rich conditions contain inclusions of the secondary Ga_2Se_3 phase. A combination of SAED and Raman spectroscopy techniques confirmed that the GaSe layers with a relatively flat surface morphology grown at T_S = 400 °C correspond to the γ-GaSe polytype, and the *c* axis of the GaSe layer in this case is normal to the substrate/layer interface. Contrary to that, GaSe layers grown at high T_S = 500 °C on the GaAs(001) substrates predominantly possess an ε-GaSe polytype, and the TEM images indicate the preferential orientation of the *c* axis of ε-GaSe along the <111> directions of the GaAs substrate due to the chemical interaction between the substrate and the growing layer. Nevertheless, the formation of a particular GaSe-polytype is governed not only by the growth temperature, but rather by a combination of various factors. The RT near band-edge excitonic photoluminescence in the GaSe/GaAs(001) layers grown at $T_S \sim$ 500 °C was demonstrated, while the intense emission band centered at ~1.7 eV dominates the PL spectra of the GaSe/GaAs(001) layers grown at low $T_S \sim$ 400 °C temperature.

The MBE growth of InSe directly on the GaAs(001) was found to be a challenge due to formation of numerous In_xSe_y-type phases in the InSe film. In the low-temperature (T = 11 K) PL spectra of InSe/GaAs(001) layers, the highest-energy peak was detected at ~1.307 eV. The temperature dependence of the PL spectrum revealed that this peak consists of the two closely-spaced and poorly separated bands, which were attributed to the recombination of native acceptor and donor–acceptor pairs, respectively. Taking account of difficulties in InSe/GaAs(001) heteroepitaxy, we tried to realize the ZnSe/InSe/ZnSe quantum well (QW) heterostructures with the thickness of InSe layers varied within 2–7 TLs range. The TEM data reveal the island character of the InSe/ZnSe(001) nucleation; however, all QW structures demonstrated the strong intense broad PL band centered at ~2.27 eV, regardless of the QW width. This PL band was associated with radiative recombination centers of In in ZnSe because of the In diffusion into the underlying ZnSe layer. In addition, the strong diffusion of Ga into the top InSe layer was observed in InSe/GaSe/GaAs(001) structures at InSe growth temperature of $T_S \sim$ 450 °C.

The near band-edge PL at T = 11 K was observed in GaTe layer grown at high $T_S \sim$ 530 °C. The peak with energy of ~1.72 eV was associated with the emission of excitons bound at the acceptor in GaTe. However, no excitonic PL was observed in the GaSe/GaTe/GaSe QW heterostructure, probably due to low growth temperature of both GaTe QW and GaSe barriers, suggesting the thesis that growth temperature is the main factor affecting the optical quality of the III–VI layers. Nevertheless, the GaSe/GaTe material system looks as the most prospective for the fabrication of the optically active QW structures due to the ability to grow the relatively flat GaTe layers at high growth temperature $T_S > 500$ °C.

and (b) cross-section TEM image, demonstrating an existence of the Ga_2Se_3 phase inclusions in the same layer, Figure S4: Cross-section TEM (a) and HRTEM (b) images of the GaSe layer grown on GaAs(001) substrate at T_S ~ 500 °C (Se/Ga(BEP) ~ 25) (sample #GS7), Figure S5: Raman spectrum of the bulk ε-GaSe layer produced by HQ Graphene—curve 1. Typical Raman spectra of γ-GaSe layers grown on GaAs(001) and GaAs(112) substrates at T_S ~ 400 °C (Curves 2 and 3, respectively). All spectra are normalized to the intensity of the A_1 (132 cm^{-1}) phonon line, Figure S6: Photoluminescence spectrum of the InSe/GaAs(001) layer measured at T = 11 K. The spectrum is most accurately approximated by four Gaussian contours centered at 1.315, 1.301, 1.28, and 1.2 eV, respectively, Figure S7: The plan-view SEM image of the InSe/GaSe/GaAs(001) structure. The growth temperature of InSe layer was as high as T_S ~ 450 °C, Figure S8: PL spectra of the GaTe/GaAs(001) layers #GT1 and #GT2 measured at the same excitation power density of 0.5 W/cm^2.

Author Contributions: Conceptualization, S.V.S.; Funding acquisition, S.V.I. and D.D.F.; Investigation, S.V.S., P.S.A., I.V.S., D.A.K., V.Y.D., O.S.K., and D.D.F.; Methodology, S.V.S., P.S.A., and V.Y.D.; Project administration, S.V.S. and S.V.I.; Supervision, S.V.S. and S.V.I.; Visualization, S.V.S., P.S.A., D.A.K., V.Y.D., O.S.K., and D.D.F.; Writing—original draft, S.V.S.; and Writing—review and editing, P.S.A., I.V.S., V.Y.D., O.S.K., D.D.F., and S.V.I. All authors have read and agreed to the published version of the manuscript.

Conflicts of Interest: The authors declare no conflict of interest. The funders had no role in the design of the study; in the collection, analyses, or interpretation of data; in the writing of the manuscript, or in the decision to publish the results.

References

1. Huang, W.; Gan, L.; Li, H.; Ma, Y.; Zhai, T. 2D layered group IIIA metal chalcogenides: Synthesis, properties and applications in electronics and optoelectronics. *CrystEngComm* **2016**, *18*, 3968–3984. [CrossRef]

2. Xu, K.; Yin, L.; Huang, Y.; Shifa, T.A.; Chu, J.; Wang, F.; Cheng, R.; Wang, Z.; He, J. Synthesis, properties and applications of 2D layered MIIIXVI(M = Ga, In; X = S, Se, Te) materials. *Nanoscale* **2016**, *8*, 16802–16818. [CrossRef] [PubMed]

3. Bandurin, D.A.; Tyurnina, A.V.; Yu, G.L.; Mishchenko, A.; Zólyomi, V.; Morozov, S.V.; Kumar, R.K.; Gorbachev, R.V.; Kudrynskyi, Z.R.; Pezzini, S.; et al. High electron mobility, quantum Hall effect and anomalous optical response in atomically thin InSe. *Nat. Nanotechnol.* **2016**, *12*, 223–227. [CrossRef] [PubMed]

4. Late, D.J.; Liu, B.; Luo, J.; Yan, A.; Matte, H.S.S.R.; Grayson, M.; Rao, C.N.R.; Dravid, V.P. GaS and GaSe Ultrathin Layer Transistors. *Adv. Mater.* **2012**, *24*, 3549–3554. [CrossRef]

5. Liu, X.; Ren, J.-C.; Shen, T.; Li, S.; Liu, W. Lateral InSe p–n Junction Formed by Partial Doping for Use in Ultrathin Flexible Solar Cells. *J. Phys. Chem. Lett.* **2019**, *10*, 7712–7718. [CrossRef]

6. Chen, Z.; Chu, S.; Chen, J.; Chen, H.; Zhang, J.; Ma, X.; Li, Q.; Chen, X. Epitaxially grown semi-vertical and aligned GaTe two dimensional sheets on ZnO substrate for energy harvesting applications. *Nano Energy* **2019**, *56*, 294–299. [CrossRef]

7. Wang, F.; Wang, Z.; Yin, L.; Cheng, R.; Wang, J.; Wen, Y.; Shifa, T.A.; Wang, F.; Zhang, Y.; Zhan, X.; et al. 2D library beyond graphene and transition metal dichalcogenides: A focus on photodetection. *Chem. Soc. Rev.* **2018**, *47*, 6296–6341. [CrossRef]

8. Yang, Z.; Hao, J. Recent Progress in 2D Layered III–VI Semiconductors and their Heterostructures for Optoelectronic Device Applications. *Adv. Mater. Technol.* **2019**, *4*, 1900108. [CrossRef]

9. Yao, J.; Zheng, Z.; Yang, G. Production of large-area 2D materials for high-performance photodetectors by pulsed-laser deposition. *Prog. Mater. Sci.* **2019**, *106*, 100573. [CrossRef]

10. Tanabe, T.; Suto, K.; Nishizawa, J.-I.; Sasaki, T. Characteristics of terahertz-wave generation from GaSe crystals. *J. Phys. D Appl. Phys.* **2003**, *37*, 155–158. [CrossRef]

11. Dong, J.; Gradwohl, K.-P.; Xu, Y.; Wang, T.; Zhang, B.-B.; Xiao, B.; Teichert, C.; Jie, W. Terahertz emission from layered GaTe crystal due to surface lattice reorganization and in-plane noncubic mobility anisotropy. *Photon. Res.* **2019**, *7*, 518–525. [CrossRef]

12. Ben Aziza, Z.; Pierucci, D.; Henck, H.; Silly, M.G.; David, C.; Yoon, M.; Sirotti, F.; Xiao, K.; Eddrief, M.; Girard, J.-C.; et al. Tunable quasiparticle band gap in few-layer GaSe/graphene van der Waals heterostructures. *Phys. Rev. B* **2017**, *96*, 035407. [CrossRef]

13. Mudd, G.W.; Molas, M.R.; Chen, X.; Zólyomi, V.; Nogajewski, K.; Kudrynskyi, Z.R.; Kovalyuk, Z.D.; Yusa, G.; Makarovsky, O.; Eaves, L.; et al. The direct-to-indirect band gap crossover in two-dimensional van der Waals Indium Selenide crystals. *Sci. Rep.* **2016**, *6*, 39619. [CrossRef] [PubMed]

14. Terry, D.J.; Zolyomi, V.; Hamer, M.J.; Tyurnina, A.V.; Hopkinson, D.; Rakowski, A.M.; Magorrian, S.; Clark, N.; Andreev, Y.M.; Kazakova, O.; et al. Infrared-to-violet tunable optical activity in atomic films of GaSe, InSe, and their heterostructures. *2D Mater.* **2018**, *5*, 041009. [CrossRef]

15. Cai, H.; Gu, Y.; Lin, Y.-C.; Yu, Y.; Geohegan, D.B.; Xiao, K. Synthesis and emerging properties of 2D layered III–VI metal chalcogenides. *Appl. Phys. Rev.* **2019**, *6*, 041312. [CrossRef]

16. Geim, A.K.; Grigorieva, I.V. Van der Waals heterostructures. *Nature* **2013**, *499*, 419–425. [CrossRef]

17. Koma, A. Van der Waals epitaxy for highly lattice-mismatched systems. *J. Cryst. Growth* **1999**, *201*, 236–241. [CrossRef]

18. Yuan, X.; Tang, L.; Wang, P.; Chen, Z.-G.; Zou, Y.-C.; Su, X.; Zhang, C.; Liu, Y.; Wang, W.; Liu, C.; et al. Wafer-scale arrayed p-n junctions based on few-layer epitaxial GaTe. *Nano Res.* **2015**, *8*, 3332–3341. [CrossRef]

19. Yuan, X.; Tang, L.; Liu, S.; Wang, P.; Chen, Z.-G.; Zhang, C.; Liu, Y.; Wang, W.; Zou, Y.; Liu, C.; et al. Arrayed van der Waals Vertical Heterostructures Based on 2D GaSe Grown by Molecular Beam Epitaxy. *Nano Lett.* **2015**, *15*, 3571–3577. [CrossRef]

20. Liu, S.; Yuan, X.; Wang, P.; Chen, Z.-G.; Tang, L.; Zhang, E.; Zhang, C.; Liu, Y.; Wang, W.; Liu, C.; et al. Controllable Growth of Vertical Heterostructure GaTexSe1–x/Si by Molecular Beam Epitaxy. *ACS Nano* **2015**, *9*, 8592–8598. [CrossRef]

21. Ueno, K.; Abe, H.; Saiki, K.; Koma, A. Heteroepitaxy of Layered Semiconductor GaSe on a GaAs(111)B Surface. *Jpn. J. Appl. Phys.* **1991**, *30*, L1352–L1354. [CrossRef]

22. Emery, J.-Y.; Brahim-Ostmane, L.; Hirlimann, C.; Chevy, A. Reflection high-energy electron diffraction studies of InSe and GaSe layered compounds grown by molecular beam epitaxy. *J. Appl. Phys.* **1992**, *71*, 3256–3259. [CrossRef]

23. Ghalouci, L.; Benbahi, B.; Hiadsi, S.; Abidri, B.; Vergoten, G.; Ghalouci, F. First principle investigation into hexagonal and cubic structures of Gallium Selenide. *Comput. Mater. Sci.* **2013**, *67*, 73–82. [CrossRef]

24. Brudnyi, V.N.; Kosobutsky, A.V.; Sarkisov, S.Y. Charge neutrality level and electronic properties of GaSe under pressure. *Semiconductors* **2010**, *44*, 1158–1166. [CrossRef]

25. Allakhverdiev, K.R.; Yetis, M.Ö.; Özbek, S.; Baykara, T.K.; Salaev, E.Y. Effective nonlinear GaSe crystal. Optical properties and applications. *Laser Phys.* **2009**, *19*, 1092–1104. [CrossRef]

26. Kuhn, A.; Chevy, A.; Chevalier, R. Crystal structure and interatomic distances in GaSe. *Phys. Status Solidi (A)* **1975**, *31*, 469–475. [CrossRef]

27. De Blasi, C.; Manno, D.; Rizzo, A. Convergent-beam electron diffraction study of melt-and vapour-grown single crystals of gallium chalcogenides. *Il Nuovo Cimento D* **1989**, *11*, 1145–1163. [CrossRef]

28. Sorokin, S.V.; Avdienko, P.S.; Sedova, I.V.; Kirilenko, D.A.; Yagovkina, M.A.; Smirnov, A.N.; Davydov, V.Y.; Ivanov, S.V. Molecular-Beam Epitaxy of Two-Dimensional GaSe Layers on GaAs(001) and GaAs(112) Substrates: Structural and Optical Properties. *Semiconductors* **2019**, *53*, 1131–1137. [CrossRef]

29. Dai, Z.; Chegwidden, S.R.; Rumaner, L.E.; Ohuchi, F.S. Microstructure evolution of GaSe thin films grown on GaAs(100) by molecular beam epitaxy. *J. Appl. Phys.* **1999**, *85*, 2603–2608. [CrossRef]

30. Lee, C.H.; Krishnamoorthy, S.; O'Hara, D.; Brenner, M.R.; Johnson, J.M.; Jamison, J.S.; Myers, R.C.; Kawakami, R.K.; Hwang, J.; Rajan, S. Molecular beam epitaxy of 2D-layered gallium selenide on GaN substrates. *J. Appl. Phys.* **2017**, *121*, 094302. [CrossRef]

31. Ueno, K.; Takeda, N.; Sasaki, K.; Koma, A. Investigation of the growth mechanism of layered semiconductor GaSe. *Appl. Surf. Sci.* **1997**, *113*, 38–42. [CrossRef]

32. Beechem, T.E.; Kowalski, B.M.; Brumbach, M.T.; McDonald, A.E.; Spataru, C.D.; Howell, S.W.; Ohta, T.; Pask, J.A.; Kalugin, N.G. Oxidation of ultrathin GaSe. *Appl. Phys. Lett.* **2015**, *107*, 173103. [CrossRef]

33. Susoma, J.; Lahtinen, J.; Kim, M.; Riikonen, J.; Lipsanen, H. Crystal quality of two-dimensional gallium telluride and gallium selenide using Raman fingerprint. *AIP Adv.* **2017**, *7*, 015014. [CrossRef]

34. Rahaman, M.; Rodriguez, R.D.; Monecke, M.; Lopez-Rivera, S.A.; Zahn, D.R.T. GaSe oxidation in air: From bulk to monolayers. *Semicond. Sci. Technol.* **2017**, *32*, 105004. [CrossRef]

35. Drapak, S.; Gavrylyuk, S.V.; Kovalyuk, Z.D.; Lytvyn, O. Native oxide emerging of the cleavage surface of gallium selenide due to prolonged storage. *Semiconductors* **2008**, *42*, 414–421. [CrossRef]

36. Han, G.; Chen, Z.-G.; Drennan, J.; Zou, J. Indium Selenides: Structural Characteristics, Synthesis and Their Thermoelectric Performances. *Small* **2014**, *10*, 2747–2765. [CrossRef]

37. Camassel, J.; Merle, P.; Mathieu, H.; Chevy, A. Excitonic absorption edge of indium selenide. *Phys. Rev. B* **1978**, *17*, 4718–4725. [CrossRef]

38. Politano, A.; Campi, D.; Cattelan, M.; Ben Amara, I.; Jaziri, S.; Mazzotti, A.; Barinov, A.; Gürbulak, B.; Duman, S.; Agnoli, S.; et al. Indium selenide: An insight into electronic band structure and surface excitations. *Sci. Rep.* **2017**, *7*, 3445. [CrossRef]

39. Hao, Q.; Yi, H.; Su, H.; Wei, B.; Wang, Z.; Lao, Z.; Chai, Y.; Wang, Z.; Jin, C.; Dai, J.; et al. Phase Identification and Strong Second Harmonic Generation in Pure ε-InSe and Its Alloys. *Nano Lett.* **2019**, *19*, 2634–2640. [CrossRef]

40. Popović, S.; Tonejc, A.; Grzeta-Plenkovic, B.; Čelustka, B.; Trojko, R. Revised and new crystal data for indium selenides. *J. Appl. Crystallogr.* **1979**, *12*, 416–420. [CrossRef]

41. Chevy, A.; Kuhn, A.; Martin, M.-S. Large InSe monocrystals grown from a non-stoichiometric melt. *J. Cryst. Growth* **1977**, *38*, 118–122. [CrossRef]

42. Nagpal, K.C.; Ali, S.Z. An X-ray study of InSe. *Indian J. Pure Appl. Phys.* **1975**, *13*, 258–264.

43. Lei, S.; Ge, L.; Najmaei, S.; George, A.; Kappera, R.; Lou, J.; Chhowalla, M.; Yamaguchi, H.; Gupta, G.; Vajtai, R.; et al. Evolution of the Electronic Band Structure and Efficient Photo-Detection in Atomic Layers of InSe. *ACS Nano* **2014**, *8*, 1263–1272. [CrossRef] [PubMed]

44. Huang, S.; Tatsumi, Y.; Ling, X.; Guo, H.; Wang, Z.; Watson, G.; Puretzky, A.A.; Geohegan, D.B.; Kong, J.; Li, J.; et al. In-Plane Optical Anisotropy of Layered Gallium Telluride. *ACS Nano* **2016**, *10*, 8964–8972. [CrossRef] [PubMed]

45. Wang, Z.; Xu, K.; Li, Y.; Zhan, X.; Safdar, M.; Wang, Q.; Wang, F.; He, J. Role of Ga Vacancy on a Multilayer GaTe Phototransistor. *ACS Nano* **2014**, *8*, 4859–4865. [CrossRef] [PubMed]

46. Kolesnikov, N.; Borisenko, E.; Borisenko, D.; Timonina, A. Structure and microstructure of GaTe crystals grown by High-Pressure vertical zone melting. *J. Cryst. Growth* **2013**, *365*, 59–63. [CrossRef]

47. Fonseca, J.J.; Tongay, S.; Topsakal, M.; Chew, A.R.; Lin, A.J.; Ko, C.; Luce, A.V.; Salleo, A.; Wu, J.; Dubon, O. Bandgap Restructuring of the Layered Semiconductor Gallium Telluride in Air. *Adv. Mater.* **2016**, *28*, 6465–6470. [CrossRef]

48. Komkov, O.S.; Firsov, D.D.; Chernov, M.Y.; Solov'Ev, V.A.; Sitnikova, A.A.; Kop'Ev, P.S.; Ivanov, S.V. Radiative versus non-radiative recombination in high-efficiency mid-IR InSb/InAs/In(Ga,Al)As/GaAs metamorphic nanoheterostructures. *J. Phys. D Appl. Phys.* **2018**, *51*, 055106. [CrossRef]

49. Kojima, N.; Sato, K.; Yamada, A.; Konagai, M.; Takahashi, K. Epitaxial Growth of GaSe Films by Molecular Beam Epitaxy on GaAs(111), (001) and (112) Substrates. *Jpn. J. Appl. Phys.* **1994**, *33*, L1482–L1484. [CrossRef]

50. Kojima, N.; Sato, K.; Budiman, M.; Yamada, A.; Konagai, M.; Takahashi, K.; Nakamura, Y.; Nittono, O. Molecular beam epitaxial growth and characterization of epitaxial GaSe films on (001)GaAs. *J. Cryst. Growth* **1995**, *150*, 1175–1179. [CrossRef]

51. Budiman, M.; Okamoto, T.; Yamada, A.; Konagai, M. Epitaxial growth and characterization of GaSxSe1−x layered compound semiconductor by molecular beam epitaxy. *Appl. Surf. Sci.* **1997**, *117*, 518–522. [CrossRef]

52. Rumaner, L.E.; Gray, J.; Ohuchi, F. Nucleation and growth of GaSe on GaAs by Van der Waal epitaxy. *J. Cryst. Growth* **1997**, *177*, 17–27. [CrossRef]

53. Rumaner, L.E. Interaction of GaSe with GaAs(111): Formation of heterostructures with large lattice mismatch. *J. Vac. Sci. Technol. B Microelectron. Nanometer Struct.* **1998**, *16*, 977. [CrossRef]

54. Novoselov, K.; Geim, A.K.; Morozov, S.; Jiang, D.; Zhang, Y.; Dubonos, S.V.; Grigorieva, I.V.; Firsov, A.A. Electric Field Effect in Atomically Thin Carbon Films. *Science* **2004**, *306*, 666–669. [CrossRef] [PubMed]

55. Diep, N.Q.; Liu, C.-W.; Wu, S.-K.; Chou, W.-C.; Huynh, S.H.; Chang, E.Y. Screw-Dislocation-Driven Growth Mode in Two Dimensional GaSe on GaAs(001) Substrates Grown by Molecular Beam Epitaxy. *Sci. Rep.* **2019**, *9*, 1–8. [CrossRef] [PubMed]

56. Ueno, K.; Sakurai, M.; Koma, A. Van der Waals epitaxy on hydrogen-terminated Si(111) surfaces and investigation of its growth mechanism by atomic force microscope. *J. Cryst. Growth* **1995**, *150*, 1180–1185. [CrossRef]

57. Nie, Y.; Barton, A.T.; Addou, R.; Zheng, Y.; Walsh, L.; Eichfeld, S.M.; Yue, R.; Cormier, C.R.; Zhang, C.; Wang, Q.; et al. Dislocation driven spiral and non-spiral growth in layered chalcogenides. *Nanoscale* **2018**, *10*, 15023–15034. [CrossRef]

58. Chen, M.; Kim, H.; Ovchinnikov, D.; Kuc, A.B.; Heine, T.; Renault, O.; Kis, A. Large-grain MBE-grown GaSe on GaAs with a Mexican hat-like valence band dispersion. *npj 2D Mater. Appl.* **2018**, *2*, 2. [CrossRef]

59. Ivanov, S.; Sorokin, S.; Sedova, I.V. *Molecular Beam Epitaxy of Wide Gap II−VI Laser Heterostructures*; Elsevier BV: Oxford, UK, 2018; Chapter 25; pp. 571–595.

60. Komkov, O.S.; Khakhulin, S.A.; Firsov, D.D.; Avdienko, P.S.; Sedova, I.V.; Sorokin, S.V. Investigation of built-in electric fields at the GaSe/GaAs interface by photoreflectance spectroscopy. *Semiconductors* **2020**, *54*, 1011–1017.

61. Dai, Z.; Ohuchi, F.S. Vacancy ordering of Ga2Se3 at GaSe/GaAs(100) interface. *Appl. Phys. Lett.* **1998**, *73*, 966–968. [CrossRef]

62. Afifi, M.; Bekheet, A.; El-Shair, H.; Zedan, I. Determination and analysis of optical constants for Ga2Se3 films near absorption edge. *Phys. B Condens. Matter* **2003**, *325*, 308–318. [CrossRef]

63. Irwin, J.; Hoff, R.; Clayman, B.; Bromley, R. Long wavelength lattice vibrations in GaS and GaSe. *Solid State Commun.* **1973**, *13*, 1531–1536. [CrossRef]

64. Hoff, R.M.; Irwin, J.C.; Lieth, R.M.A. Raman Scattering in GaSe. *Can. J. Phys.* **1975**, *53*, 1606–1614. [CrossRef]

65. Lim, S.Y.; Lee, J.-U.; Kim, J.H.; Liang, L.; Kong, X.; Nguyen, T.T.H.; Lee, Z.; Cho, S.; Cheong, H. Polytypism in few-layer gallium selenide. *Nanoscale* **2020**, *12*, 8563–8573. [CrossRef]

66. Yoshida, H.; Nakashima, S.; Mitsuishi, A. Phonon Raman spectra of layer compound GaSe. *Phys. Status Solidi (B)* **1973**, *59*, 655–666. [CrossRef]

67. Bergeron, A.; Ibrahim, J.; Leonelli, R.; Francoeur, S. Oxidation dynamics of ultrathin GaSe probed through Raman spectroscopy. *Appl. Phys. Lett.* **2017**, *110*, 241901. [CrossRef]

68. Longuinhos, R.; Ribeiro-Soares, J.; Longuinhos, R. Ultra-weak interlayer coupling in two-dimensional gallium selenide. *Phys. Chem. Chem. Phys.* **2016**, *18*, 25401–25408. [CrossRef]

69. Polian, A.; Kunc, K.; Kuhn, A. Low-frequency lattice vibrations of δ-GaSe compared to ε- and γ-polytypes. *Solid State Commun.* **1976**, *19*, 1079–1082. [CrossRef]

70. Zhou, J.; Wu, Y.; Wang, H.; Wu, Z.; Li, X.; Yang, W.; Ke, C.; Lu, S.; Zhang, C.; Kang, J.; et al. Strain manipulation of the polarized optical response in two-dimensional GaSe layers. *Nanoscale* **2020**, *12*, 4069–4076. [CrossRef]

71. Cai, H.; Soignard, E.; Ataca, C.; Chen, B.; Ko, C.; Aoki, T.; Pant, A.; Meng, X.; Yang, S.; Grossman, J.; et al. Band Engineering by Controlling vdW Epitaxy Growth Mode in 2D Gallium Chalcogenides. *Adv. Mater.* **2016**, *28*, 7375–7382. [CrossRef]

72. Capozzi, V.; Montagna, M. Optical spectroscopy of extrinsic recombinations in gallium selenide. *Phys. Rev. B* **1989**, *40*, 3182–3190. [CrossRef] [PubMed]

73. Budiman, M.; Yamada, A.; Konagai, M. Heteroepitaxy of Layered Compound InSe and InSe/GaSe onto GaAs Substrates. *Jpn. J. Appl. Phys.* **1998**, *37*, 4092–4098. [CrossRef]

74. Capozzi, V. Direct and indirect excitonic emission in GaSe. *Phys. Rev. B* **1981**, *23*, 836–840. [CrossRef]

75. Avdienko, P.; Sorokin, S.; Sedova, I.; Kirilenko, D.; Smirnov, A.; Eliseev, I.; Davydov, V.; Ivanov, S. Structural and Optical Properties of GaSe/GaAs(001) Layers Grown by Molecular Beam Epitaxy. *Acta Phys. Pol. A* **2019**, *136*, 608–612. [CrossRef]

76. Chatillon, C. Critical analysis of the thermodynamic properties of the In-Se gaseous and solid phases. *J. Cryst. Growth* **1993**, *129*, 297–311. [CrossRef]

77. Emery, J.; Julien, C.; Jouanne, M.; Balkanski, M. Growth conditions and structure of polycrystalline InSe thin films. *Appl. Surf. Sci.* **1988**, *33*, 619–624. [CrossRef]

78. Emery, J.; Brahim-Otsmane, L.; Jouanne, M.; Julien, C.; Balkanski, M. Growth conditions of films by molecular beam deposition. *Mater. Sci. Eng. B* **1989**, *3*, 13–17. [CrossRef]

79. Brahim-Otsmane, L.; Emery, J.-Y.; Eddrief, M. X-ray, reflection high electron energy diffraction and X-ray photoelectron spectroscopy studies of InSe and γ-In2Se3 thin films grown by molecular beam deposition. *Thin Solid Films* **1994**, *237*, 291–296. [CrossRef]

80. Jasinski, J.; Liliental-Weber, Z.; Chaiken, A.; Gibson, G.; Nauka, K.; Yang, C.; Bicknell, R. Heteroepitaxy of InSe/GaSe on Si(111) Substrates. *MRS Symp. Proc.* **2003**, *803*. [CrossRef]

81. Chatillon, C.; Emery, J.-Y. Thermodynamic analysis of molecular beam epitaxy of compounds in the In-Se system. *J. Cryst. Growth* **1993**, *129*, 312–320. [CrossRef]

82. Ivanov, S.; Sorokin, S.; Kop'Ev, P.; Kim, J.; Jung, H.; Park, H. Composition, stoichiometry and growth rate control in molecular beam epitaxy of ZnSe based ternary and quaternary alloys. *J. Cryst. Growth* **1996**, *159*, 16–20. [CrossRef]

83. Ivanov, S.; Sorokin, S.; Krestnikov, I.; Faleev, N.; Ber, B.; Sedova, I.; Kudryavtsev, Y.; Kop'Ev, P. Interplay of kinetics and thermodynamics in molecular beam epitaxy of (Mg,Zn,Cd)(S,Se). *J. Cryst. Growth* **1998**, *184*, 70–74. [CrossRef]

84. Julien, C.; Khelfa, A.; Benramdane, N.; Guesdon, J. Preparation and characterization of In4Se3 films. *Mater. Sci. Eng. B* **1994**, *27*, 53–60. [CrossRef]

85. Zhai, Y.; Zhang, Q.; Jiang, J.; Zhang, T.; Xiao, Y.; Yang, S.; Xu, G. Thermoelectric performance of the ordered In4Se3–In composite constructed by monotectic solidification. *J. Mater. Chem. A* **2013**, *1*, 8844. [CrossRef]

86. Milutinović, A.; Lazarević, Z.Ž.; Jakovljević, M.; Hadzić, B.; Petrović, M.; Gilić, M.; Dobrowolski, W.D.; Romčević, N.Ž. Optical properties of layered III–VI semiconductor γ -InSe: M (M = Mn, Fe, Co, Ni). *J. Phys. Chem. Solids* **2016**, *89*, 120–127. [CrossRef]

87. Carlone, C.; Jandl, S.; Shanks, H.R. Optical Phonons and Crystalline Symmetry of InSe. *Phys. Status Solidi (B)* **1981**, *103*, 123–130. [CrossRef]

88. Segura, A. Layered Indium Selenide under High Pressure: A Review. *Crystals* **2018**, *8*, 206. [CrossRef]

89. Wu, M.; Xie, Q.; Wu, Y.; Zheng, J.; Wang, W.; He, L.; Wu, X.; Lv, B. Crystal structure and optical performance in bulk γ-InSe single crystals. *AIP Adv.* **2019**, *9*, 025013. [CrossRef]

90. Grimaldi, I.; Gerace, T.; Pipita, M.; Perrotta, I.; Ciuchi, F.; Berger, H.; Papagno, M.; Castriota, M.; Pacilé, D. Structural investigation of InSe layered semiconductors. *Solid State Commun.* **2020**, *311*, 113855. [CrossRef]

91. Kuroda, N.; Nishina, Y. Resonant Raman scattering at higher M0 exciton edge in layer compound InSe. *Solid State Commun.* **1978**, *28*, 439–443. [CrossRef]

92. Otsmane, L.B.; Emery, J.; Jouanne, M.; Balkanski, M. Epitaxy of layered semiconductor thin films. *Appl. Surf. Sci.* **1993**, *65*, 479–481. [CrossRef]

93. Hayashi, T.; Ueno, K.; Saiki, K.; Koma, A. Investigation of the growth mechanism of an InSe epitaxial layer on a MoS2 substrate. *J. Cryst. Growth* **2000**, *219*, 115–122. [CrossRef]

94. Shubina, T.V.; Desrat, W.; Moret, M.; Tiberj, A.; Briot, O.; Davydov, V.Y.; Platonov, A.; Semina, M.A.; Gil, B. InSe as a case between 3D and 2D layered crystals for excitons. *Nat. Commun.* **2019**, *10*, 3479. [CrossRef] [PubMed]

95. Abha Photoluminescence studies on the layer semiconductor InSe. *J. Appl. Phys.* **1982**, *53*, 5169. [CrossRef]

96. Abay, B.; Efeoğlu, H.; Yoğurtçu, Y. Low-temperature photoluminescence of n-InSe layer semiconductor crystals. *Mater. Res. Bull.* **1998**, *33*, 1401–1410. [CrossRef]

97. Homs, A.A.; Marí, B. Photoluminescence of undoped and neutron-transmutation-doped InSe. *J. Appl. Phys.* **2000**, *88*, 4654. [CrossRef]

98. Lang, O.; Klein, A.; Schlaf, R.; Löher, T.; Pettenkofer, C.; Jaegermann, W.; Chevy, A. heterointerfaces prepared by Van der Waals epitaxy. *J. Cryst. Growth* **1995**, *146*, 439–443. [CrossRef]

99. Royo, J.F.S.; Segura, A.; Lang, O.; Pettenkofer, C.; Jaegermann, W.; Chevy, A.; Roa, L. Photovoltaic properties of indium selenide thin films prepared by van der Waals epitaxy. *Thin Solid Films* **1997**, *307*, 283–287. [CrossRef]

100. Wisotzki, E.; Klein, A.; Jaegermann, W. Quasi van der Waals epitaxy of ZnSe on the layered chalcogenides InSe and GaSe. *Thin Solid Films* **2000**, *380*, 263–265. [CrossRef]

101. Avdienko, P.S.; Kirilenko, D.A.; Sedova, I.V.; Sorokin, S.V. Structural properties of ZnSe/InSe/ZnSe heterostructures grown by molecular beam epitaxy on GaAs(001) substrates. *J. Physics Conf. Ser.* **2020**, *1482*, 012006. [CrossRef]

102. Smathers, J.B.; Kneedler, E.; Bennett, B.; Jonker, B. Nanometer scale surface clustering on ZnSe epilayers. *Appl. Phys. Lett.* **1998**, *72*, 1238–1240. [CrossRef]

103. Qidwai, A.; Woods, J. Defect levels in indium and gallium doped zinc selenide. *J. Cryst. Growth* **1982**, *59*, 217–222. [CrossRef]

104. Isshiki, M.; Yoshida, T.; Igaki, K.; Hayashi, Y.; Nakano, Y. Photoluminescence spectra of In-doped ZnSe single crystals. *J. Phys. C Solid State Phys.* **1986**, *19*, 4375–4381. [CrossRef]

105. Antonopoulos, J.G.; Karakostas, T.; Bleris, G.L.; Economou, N.A. On the phase diagram of the Ga-Te system in the composition range 55 at % Te. *J. Mater. Sci.* **1981**, *16*, 733–738. [CrossRef]

106. Teraguchi, N.; Kato, F.; Konagai, M.; Takahashi, K. Growth of III-VI Compound Semiconductors by Metalorganic Molecular Beam Epitaxy. *Jpn. J. Appl. Phys.* **1989**, *28*, L2134–L2136. [CrossRef]

107. Teraguchi, N.; Kato, F.; Konagai, M.; Takahashi, K. Growth and characterization of Ga2Te3 films by metalorganic molecular beam epitaxy. *J. Electron. Mater.* **1991**, *20*, 247–250. [CrossRef]

108. Bae, C.J.; McMahon, J.; Detz, H.; Strasser, G.; Park, J.; Einarsson, E.; Eason, D. Influence of thickness on crystallinity in wafer-scale GaTe nanolayers grown by molecular beam epitaxy. *AIP Adv.* **2017**, *7*, 35113. [CrossRef]

109. Zhao, Q.; Wang, T.; Miao, Y.; Ma, F.; Xie, Y.; Ma, X.; Gu, Y.; He, J.; Chen, B.; Xi, S.; et al. Thickness-induced structural phase transformation of layered gallium telluride. *Phys. Chem. Chem. Phys.* **2016**, *18*, 18719–18726. [CrossRef]

110. Borisenko, E.; Borisenko, D.; Timonina, A.; Kolesnikov, N. Nonvariant polymorphic transition from hexagonal to monoclinic lattice in GaTe single crystal. *J. Cryst. Growth* **2020**, *535*, 125548. [CrossRef]

111. Liu, F.; Shimotani, H.; Shang, H.; Kanagasekaran, T.; Zólyomi, V.; Drummond, N.D.; Fal'Ko, V.I.; Tanigaki, K. High-Sensitivity Photodetectors Based on Multilayer GaTe Flakes. *ACS Nano* **2014**, *8*, 752–760. [CrossRef]

112. Yu, Y.; Ran, M.; Zhou, S.; Wang, R.; Zhou, F.; Li, H.; Gan, L.; Zhu, M.; Zhai, T. Phase-Engineered Synthesis of Ultrathin Hexagonal and Monoclinic GaTe Flakes and Phase Transition Study. *Adv. Funct. Mater.* **2019**. [CrossRef]

113. Gillan, E.G.; Barron, A.R. Chemical Vapor Deposition of Hexagonal Gallium Selenide and Telluride Films from Cubane Precursors: Understanding the Envelope of Molecular Control. *Chem. Mater.* **1997**, *9*, 3037–3048. [CrossRef]

114. Güder, H.; Abay, B.; Efeoğlu, H.; Yoğurtçu, Y.; Efeoğlu, H.; Yoğurtçu, Y. Photoluminescence characterization of GaTe single crystals. *J. Lumin.* **2001**, *93*, 243–248. [CrossRef]

115. Zubiaga, A.; García, J.A.; Plazaola, F.; Muñoz-Sanjose, V.; Martínez-Tomás, M.C. Recombination processes in unintentionally doped GaTe single crystals. *J. Appl. Phys.* **2002**, *92*, 7330–7336. [CrossRef]

116. Fonseca, J.J.; Horton, M.K.; Tom, K.; Yao, J.; Walukiewicz, W.; Dubón, O.D. Structure–Property Relationship of Low-Dimensional Layered GaSexTe1−x Alloys. *Chem. Mater.* **2018**, *30*, 4226–4232. [CrossRef]

117. Cai, H.; Chen, B.; Blei, M.; Chang, L.Y.; Wu, K.; Zhuang, H.; Tongay, S. Abnormal band bowing effects in phase instability crossover region of GaSe1-xTe x nanomaterials. *Nat. Commun.* **2018**, *9*, 1927. [CrossRef]

118. Cai, H.; Chen, B.; Wang, G.; Soignard, E.; Khosravi, A.; Manca, M.; Marie, X.; Chang, S.L.Y.; Urbaszek, B.; Tongay, S. Synthesis of Highly Anisotropic Semiconducting GaTe Nanomaterials and Emerging Properties Enabled by Epitaxy. *Adv. Mater.* **2016**, *29*, 1605551. [CrossRef]

119. Williams, E.W.; Bebb, H.B. Photoluminescence II: Gallium Arsenide. In *Semiconductors and Semimetals*; Willardson, R.K., Beer, A.C., Eds.; Academic Press: New York, NY, USA, 1972; Volume 8, Chapter 5; pp. 321–392.

120. Cai, H.; Kang, J.; Sahin, H.; Chen, B.; Suslu, A.; Wu, K.; Peeters, F.; Meng, X.; Tongay, S. Exciton pumping across type-I gallium chalcogenide heterojunctions. *Nanotechnology* **2016**, *27*, 065203. [CrossRef]